CIMMS Report No. 71

Characteristics of Echoes from Alternately Polarized Transmission

by

M. Sachidananda

Cooperative Institute for Mesoscale Meteorological Studies

University of Oklahoma

and

D.S. Zrnić

National Severe Storms Laboratory

ERL, NOAA

July 1986

Cooperative Institute for Mesoscale Meteorological Studies

401 East Boyd, Norman, Oklahoma 73019

Characteristics of Echoes from Alternately Polarized Transmission

M. Sachidananda and D.S. Zrnić

Contents

PREFACE

Dr. Sachidananda, the first author of this report, was a postdoctoral fellow at CIMMS when this research was performed. He and Dr. Zrnić have collaborated on several aspects of polarization studies including: 1) efficient methods of estimating differential phase shift and differential reflectivity, 2) statistics of differential polarization measurements, 3) rain rate estimation from differential phase measurements and 4) data analysis. These topics have found their way into open literature. However certain relevent ideas and latest results of data analysis were confined to the authors and their desks. Because polarization measurements with weather radars is an active field of research and because the National Severe Storms Laboratory radar has a unique capability to record time series data of alternately polarized echoes, the authors have decided to collect their notes into a report. Alternating, horizontally and vertically polarized signals are a common thread that joins these notes for the purpose to concisely and in one place document the authors work and to share it with others that have interest in weather radar polarimetry.

We appreciate the support given to us by both CIMMS and NSSL during the course of this work. Special thanks go to Dr. Sasaki who arranged for the postdoctoral postion, to Mr. Sirmans who was responsible for polarization incorporation and operation of the radar and to Dr. Doviak who reviewed the manuscript.

Characteristics of Echoes from Alternately Polarized Transmission

M. Sachidananda and D.S. Zrnić

1. Introduction

The differential reflectivity (Z_{DR}) measurement advanced by Seliga and Bringi [1976] has generated considerable interest among radar meteorologists as evidenced by a large number of research publications. This is not suprising since the measurement has potential to improve the accuracy of radar rain rate estimation. Furthermore polarization diversity may lead to remote methods of hydrometeor identification in storms as evidenced by recent results of successful hail detection. Several research radars with dual linear polarization capability have been built since; most recent among them is the NSSL's radar facility at Cimarron. The capability of NSSL radar system to record complex echo sample time-series has made it possible to estimate the differential propagation phase shift (ϕ_{DP}) in addition to the differential reflectivity; though not in real time.

A single polarized Doppler weather radar generally estimates first three spectral moments of the echo signal from which the three commonly used radar observables, namely the reflectivity (Z), the velocity (v) and the spectrum width (σ_v) are derived. Whereas the reflectivity is roughly proportional to the intensity of rainfall in the radar resolution volume, accurate estimation of the rainfall rate entails knowledge of the drop size distribution (DSD). Because of the large variability in the DSD in natural rain, a simple Z-R relation based on an assumed exponential DSD shape has met with limited success when determining the rainfall rate with the same spatial and temporal resolution as the reflectivity measurement.

The fact that raindrops, falling with the terminal velocity, have a definite axis ratio (b/a) versus equivolumetric diameter (D_e) relation, has lead to the possibility of estimating the DSD via the measurement of differential backscatter properties of drops. The primary motivation for developing radars with Z_{DR} measurement capability has been the possibility of accurate rainfall rate estimation with high spatial and temporal resolution. Other uses of the Z_{DR} in identifying hail and melting layer have been recognized later.

A more recent development is the measurement of the differential propagation phase shift constant K_{DP}, (Sachidananda and Zrnić, 1986). Theoretical analysis showed that simple $R(K_{DP})$ relation is much less sensitive to DSD variation than a $R(Z)$ or a $R(Z_H/Z_{DR})$ relation and thus should give accurate rainfall rate estimates. First estimates of K_{DP} have shown that it is plagued by various measurement errors which limit its usefulness to very high rainfall rates. The spatial distribution of K_{DP} estimates shows that there is a significant information content in the K_{DP} data field. One of the possible uses of differential phase measurement would be for rainfall rate integration over an area. Because the total differential phase shift (ϕ_{DP}) is inherently an integral over the path length, we need to estimate ϕ_{DP} only at two points along a radial from which the integral of the rainfall rate along the path between the two points can be determined.

A dual polarized radar designed for Z_{DR} measurement consists of a polarization switch added to a conventional single polarized radar system. Vertically and horizontally polarized pulses are transmitted alternately and only co-polar signals are received, allowing measurements only of the diagonal terms in the back-scattering matrix. The Z_{DR} is the ratio of mean sample powers received in the horizontal and vertical polarizations. It is not necessary that the radar be coherent for Z_{DR} measurement but for Doppler velocity and ϕ_{DP} measurement, coherency is required.

Because the rain drops are oblate and nearly oriented with the axis of symmetry along the vertical, radar crosssection is different for the two polarizations and so is the propagation constant through the rain medium. This reflects as an amplitude and phase modulation of the time series samples at the polarization switching frequency. The amplitude modulation index can be related to the Z_{DR} and the phase modulation to ϕ_{DP}. Weather signals generally have spectra which can be approximated to a Gaussian shape. Due to the polarization switching and the consequent modulation, the spectrum of radar signal with alternating polarization exhibits two peaks separated by half the Nyquist interval. This necessitates some modifications in the normally used computational procedure for the estimation of the reflectivity, the velocity and the spectrum width.

The estimation of spectral moments for a single polarized radar has been well documented elsewhere (Doviak and Zrnić, 1984). This report primarily addresses the modification in those standard procedures necessitated by the polarization switching.

2. Radar echo signal with alternating polarization:

A pulsed Doppler radar system samples the echo signal at a fixed delay time after a pulse is transmitted. The sample voltage is a composite of the backscattered signals from all the scatterers in the resolution volume and the range to the resolution volume is obtained from the delay time. Representing the sample voltages for the horizontally and the vertically polarized transmission by H and V respectively, we can express the n^{th} sample (H) and the $(n + 1)^{th}$ sample (V) as a summation of back-scattered signals from all scatters in the resolution volume.

$$H_n = K \sum_i s_h^i I^i \exp [-j\gamma_h^i(n)] \qquad (1.a)$$

$$V_{n+1} = K \sum_i s_v^i I^i \exp [-j\gamma_v^i(n+1)] \qquad (1.b)$$

where $$\gamma^{i}_{h,v}(n) = 2(k_o + k_{h,v})r_{n,i} \qquad (2.a)$$

$$\gamma^{i}_{h,v}(n+1) = 2(k_o + k_{h,v})r_{n,i} + 2(k_o + k_{h,v})T_s v_i \qquad (2.b)$$

The summation index refers to the i^{th} scatterer and the summation is over all scatterers in the resolution volume. The subscripts h,v refer to the horizontal and the vertical polarization respectively. T_s is pulse repetition time, K is a constant dependent on radar parameters, $s^{i}_{h,v}$ are the diagonal elements of the backscattering matrix and I_i is the illumination function which contains the initial transmitter phase ψ_i. The propagation constants for vertically and horizontally polarized fields are represented by $(k_o + k_h)$ and $(k_o + k_v)$ respectively, with k_o as the free space propagation constant. The range to the i^{th} scatterer at time (nT_s) is represented by $r_{n,i}$, and the average radial velocity of the i^{th} scatter in the time interval $(nT_s,(n+1)T_s)$ by v_i, so that $r_{n+1,i} = r_{n,i} + T_s v_i$. Although $\gamma^{i}_{h,v}$ are complex, the imaginary part, which gives rise to attenuation along the propagation path, is small at S-band frequencies, hence, is neglected in our subsequent calculations.

Basically a sequence of these samples, known as the time series, is all that a radar provides, for each resolution volume and all the information about the scatterers in the resolution volume is derived from it. In a single polarized radar the most important meteorological information is obtained from the first three moments of the Fourier transform i.e. the Doppler spectrum of this time series. The reflectivity is calculated from the mean sample power or the zeroth moment, mean radial velocity from the first moment of the normalized power spectrum and the spectrum width, which is a measure of the turbulence and/or shear in the resolution volume, is the square root of the second moment of the Doppler spectrum about the mean radial velocity.

Because of the statistical nature of weather echoes, one needs to obtain estimates of spectral moments using several samples. The mean sample power S is estimated using

$$\hat{S} = \frac{1}{M} \sum_{i} |E_i|^2 \qquad (3)$$

where M is the number of samples averaged, and E_i are echo sample voltages (either H or V samples). To accomodate the large dynamic range of echo strengths, a logarithmic receiver is used and the samples obtained from the log receiver are integrated to estimate the mean echo power (Fig. 1). The output of the integrator is also used to control the gain of a linear receiver channel from which complex time series samples are obtained.

The linear receiver output is made nearly constant by AGC voltage derived from the log-receiver output. This is necessary to keep the output within the dynamic range of the analog to digital converter. The output of the linear IF channel is demodulated in a quadrature receiver and is sampled and digitized to obtain in-phase (I) and quadrature-phase (Q) components of the sample (Fig. 1). When these samples are used for calculating the reflectivity it is required to calibrate each gate (both I and Q channels). If a mean calibration curve is used, the estimated mean sample power can be in error by as much as ±3dB. A simple way is to determine the gain of I and Q channels for each gate as a function of AGC voltage. It is common practice to use discrete AGC levels (64 levels) thus, only a fixed number of gain readings need be stored for use in the reflectivity calculation.

The mean radial velocity and spectrum width can be estimated using autocovariance processing, which is simpler computationally and cost-wise, than the spectral processing. In the autocovariance method the mean velocity is given by

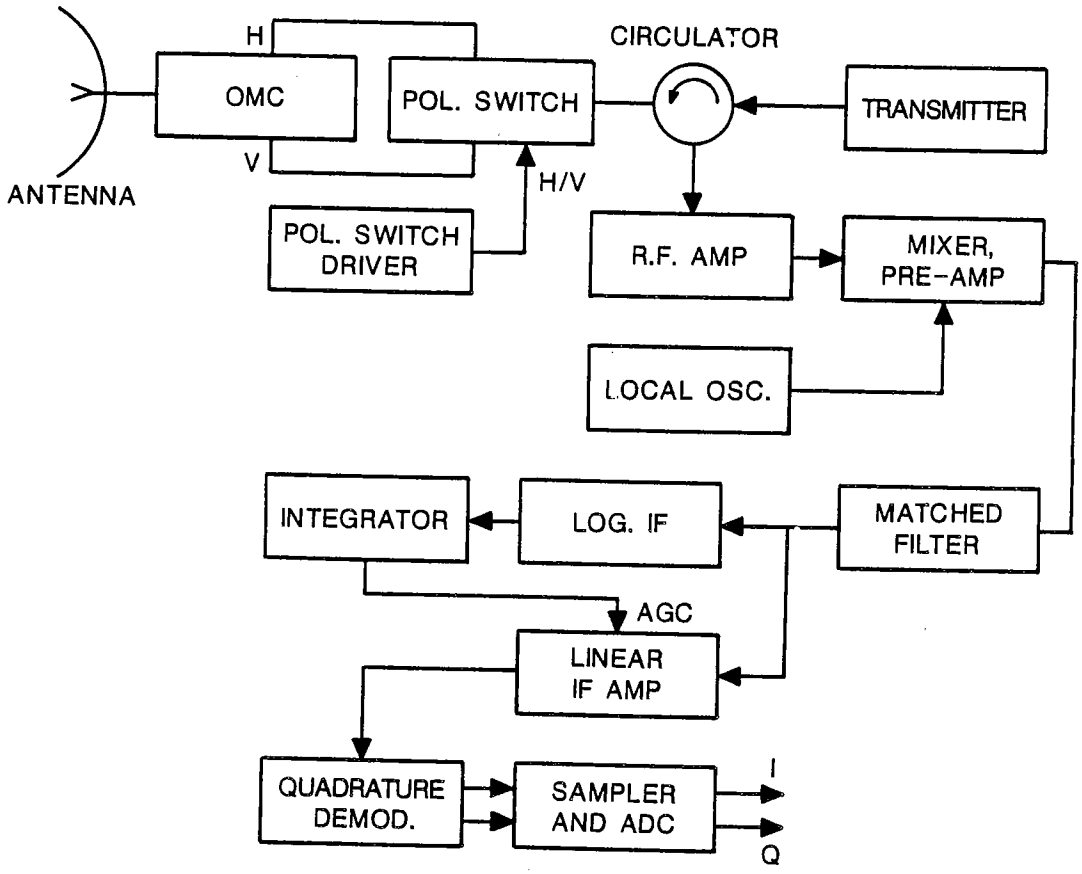

Figure 1. Schematic of a Doppler radar that can transmit signals with alternating polarization.

$$\hat{v} = -(\lambda/4\pi T_s)\arg[\hat{R}(T_s)] \tag{4}$$

where the autocorrelation estimate $\hat{R}(T_s)$ for lag time T_s is

$$\hat{R}(T_s) = \frac{1}{M}\sum_{i=1}^{M} E_i^* E_{i+1}. \tag{5}$$

The spectrum width is also calculated from $\hat{R}(T_s)$ and $\hat{S}$ using

$$\hat{\sigma}_v = \frac{\sqrt{2}\cdot v_a}{\pi}\left|\ln\left(\frac{\hat{S}}{|\hat{R}|}\right)\right|^{1/2}\operatorname{sgn}\left[\ln\left(\frac{\hat{S}}{|\hat{R}|}\right)\right] \tag{6}$$

where v_a is the Nyquist velocity equal to λ/T_s. A detailed treatment of estimators of Z, v and σ_v and their standard errors, is given in Doviak and Zrnić (1984).

A dual linear polarized radar provides two more parameters of interest to the meteorologist. They are the differential reflectivity (Z_{DR}) and the differential propagation phase shift (ϕ_{DP}). The alternate polarization switching, which enables us to estimate these two additional polarization dependent parameters, also affects the estimation of the three conventional parameters. In the following the estimation of each of these five radar observables using the dual polarized radar, is discussed.

3. Estimation of Radar Observables:

3.1. Reflectivity and differential reflectivity:

The primary intended use of the Z_{DR} is for accurate rainfall estimation. To estimate the rainfall rate more accurately using the Z_{DR}-method, than that given by a R(Z) relation, it is required to estimate Z_{DR} to an accuracy of 0.1 dB and the reflectivity for the horizontally polarized field (Z_H), to an accuracy of 1 dBZ (Sachidananda and Zrnić, 1985). So, the number of samples required is dictated by these accuracy requirements. Figures 2 and 3 show the standard errors

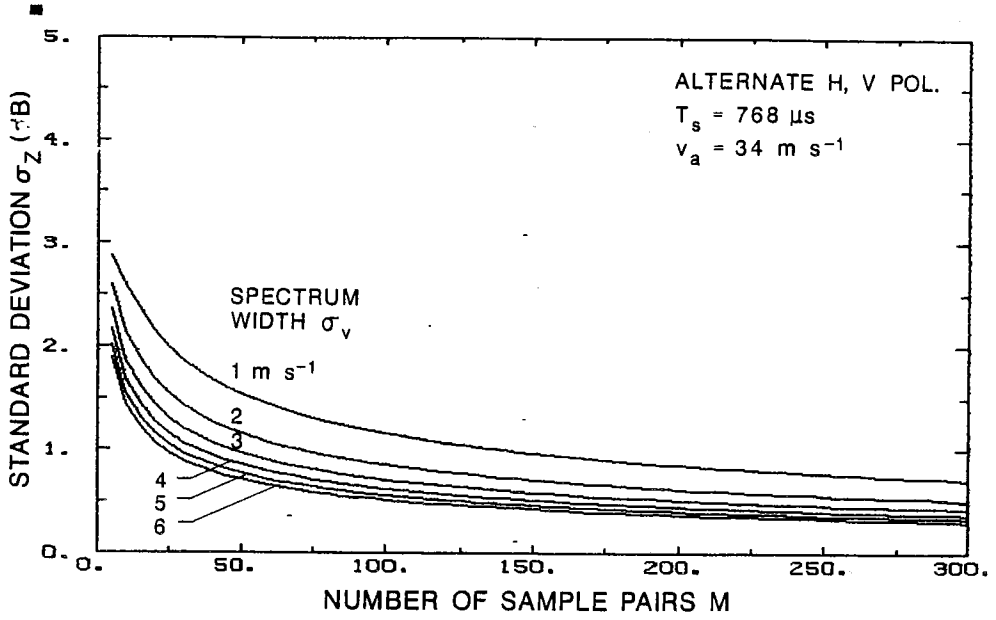

Figure 2. Standard error of Z_H estimates. Because this graph is for alternate samples the number of sample pairs equals to the number of reflectivity samples at horizontal or vertical polarization.

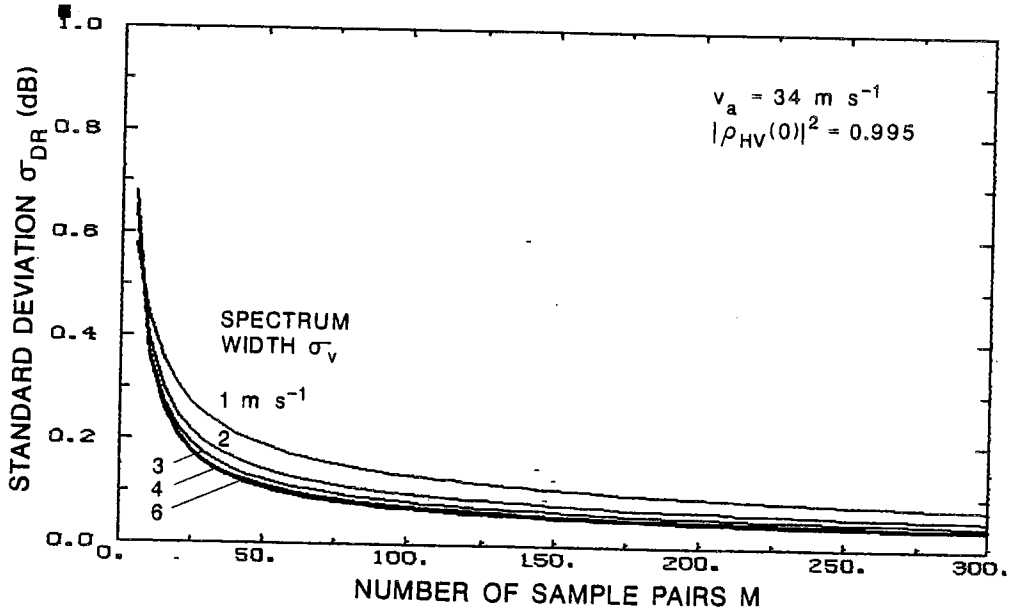

Figure 3. Standard error of Z_{DR} estimates.

σ_z and σ_{DR} in $\hat{Z}_H$ and $\hat{Z}_{DR}$ estimates respectively, as a function of the number of samples averaged. The spectrum width of the signal is shown as a parameter. It is obvious from a comparison of these two figures that the standard error in Z_{DR} dictates the number of samples required for improved rain rate estimation.

The mean sample powers $\hat{S}_H$ and $\hat{S}_V$ for the two polarizations have to be calculated separately to estimate Z_{DR}. If samples from the linear receiver are used, Z_H and Z_{DR} are estimated from

$$\hat{S}_H = \frac{1}{M} \sum_{i=1}^{M} |H_{2i}|^2 \tag{7}$$

$$\hat{S}_V = \frac{1}{M} \sum_{i=1}^{M} |V_{2i+1}|^2 \tag{8}$$

and

$$\hat{Z}_{DR} = 10 \log \left(\frac{\hat{S}_H}{\hat{S}_V}\right) \quad \text{(dB)} \tag{9}$$

Here, M is the number of sample pairs. It may be noted that the number of samples available for $\hat{S}_H$ or $\hat{S}_V$ estimation is half that available in a single polarized radar, in the same time interval. However, the increase in the standard error due to this reduced number is usually insignificant because, for a sufficiently large M, the standard error is a function of the total sampling time and the decorrelation time of the signal, which remain unaltered.

An alternate way to implement Z_{DR} estimation is to separate H and V samples from the log-receiver and integrate them to obtain Z_H and Z_V. This procedure has the disadvantage of an increased standard error by a factor of about 2 in the $\hat{Z}_{DR}$ (Bringi et al, 1983), which necessitates further increase in the number of sample pairs M. The square law estimator (eqns. 7, 8, 9) has the lowest standard error, thus, in view of the faster scan rate requirements to keep the data update time small, it would be desirable to implement the square law estimator. The log-receiver and integrators may still be required to obtain the gain control voltage for the linear channels or other methods for gain control must be employed.

If the antenna patterns and the transmitted powers in the two polarizations were perfectly matched, the $\hat{Z}_{DR}$ would not have any bias eror. But, accurate calibration is required for the $\hat{Z}_H$, because both $\hat{Z}_H$ and $\hat{Z}_{DR}$ are used in R estimation. It is normal practice to use a mean calibration curve for all integrator samples, in the calculation of the reflectivity factor. On the CIM radar the receiver gains for each of the sixteen range gates may be different. Although this difference was found to be less than 2 dB we have used individual calibration curves for each range gate. The output itself is quantized at approximately 1 dB intervals. Thus, the reflectivity estimates would have a quantization error and could have a calibration error due to the variations in the individual integrator channel gains about the mean calibration. These errors become particularly important for R estimation, and have to be reduced by increasing the number of quantization levels and if needed by using individual calibration curves for each range gate.

The calibration procedure steps the AGC amplifiers control voltage through all the levels and records M number of I and Q samples for each gate and for each AGC level. From this record we can calculate the gain of each I and Q channel for each range gate. In the calibration record, let P_n(mW) be the input power, I'_i and Q'_i are the i^{th} digitized sample components and A_n the AGC number. According to the statistical properties of I and Q samples, their mean value is zero, and if a dc component is present in the measured sample values it would be due to the amplifier dc offset or ground clutter. So, first the dc bias is removed from the I and Q samples. The corrected set of samples are:

$$I_i = I'_i - \frac{1}{M}\sum_{i=1}^{M} I'_i$$
$$Q_i = Q'_i - \frac{1}{M}\sum_{i=1}^{M} Q'_i \qquad (10)$$

The power gain of each channel can be calculated as:

$$G_I(A_n) = \frac{2}{MP_n} \sum_{i=1}^{M} I_i^2$$
$$G_Q(A_n) = \frac{2}{MP_n} \sum_{i=1}^{M} Q^2{}_i \qquad (11)$$

These gain calibration values are stored in the computer memory and used in estimating the received mean sample power P_r:

$$P_r = \frac{1}{M} \frac{\sum I_i{}^2}{G_I} + \frac{\sum Q_i{}^2}{G_Q} \quad (mW) \qquad (12)$$

When polarization is switched between the horizontal and the vertical directions, I_H, Q_H and I_V,Q_V samples are processed separately for dc removal. It may be noted that because H and V samples individually have a repetition time equal to $2T_s$, the Nyquist component also gets eliminated in the process of dc removal.

3.2 Mean radial velocity and differential propagation phase shift:

The mean radial velocity and the differential propagation phase shift are obtained from phases of the received echo samples. The weather echo sample spectra can be approximated by a Gaussian shape in most cases. For such spectra the mean radial velocity, v, and the spectrum width σ_v, are estimated using the autocovariance and the mean sample power estimates (eqns. 4, 6). Estimators (4) and (8) do not perform satisfactorily when applied to alternately polarized radar signals. The reason for this is clear from an examination of the Doppler spectra of these signals. In figure 4 a typical spectrum obtained from the time series record of the NSSL's dual polarized radar is shown. The echo is from a region of high reflectivity and large signal to noise ratio (SNR > 20 dB) so that the weather spectral powers are well above the nearly zero noise level. The number of samples used for FFT is 256 and the magnitudes of the Fourier coefficients are plotted on a normalized linear vertical scale.

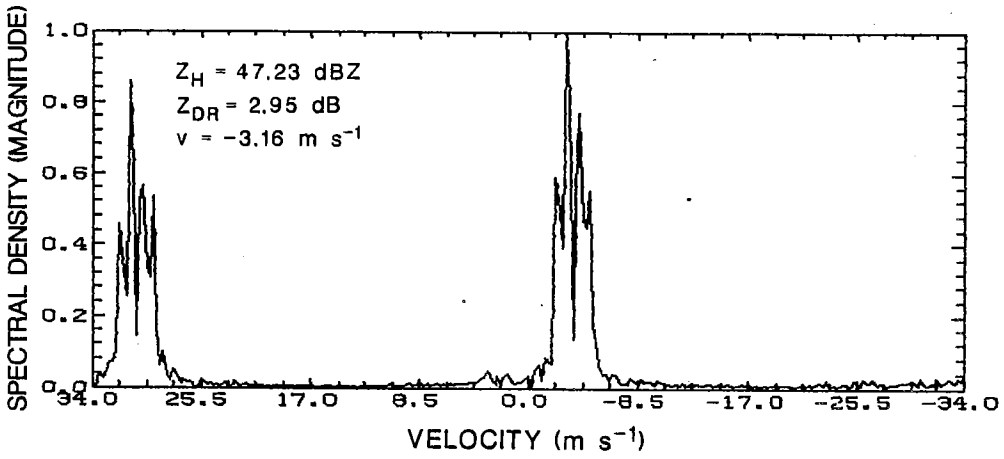

Figure 4. Normalized Doppler spectrum of a signal with alternate polarization. Positive phase shift correspond to negative velocities.

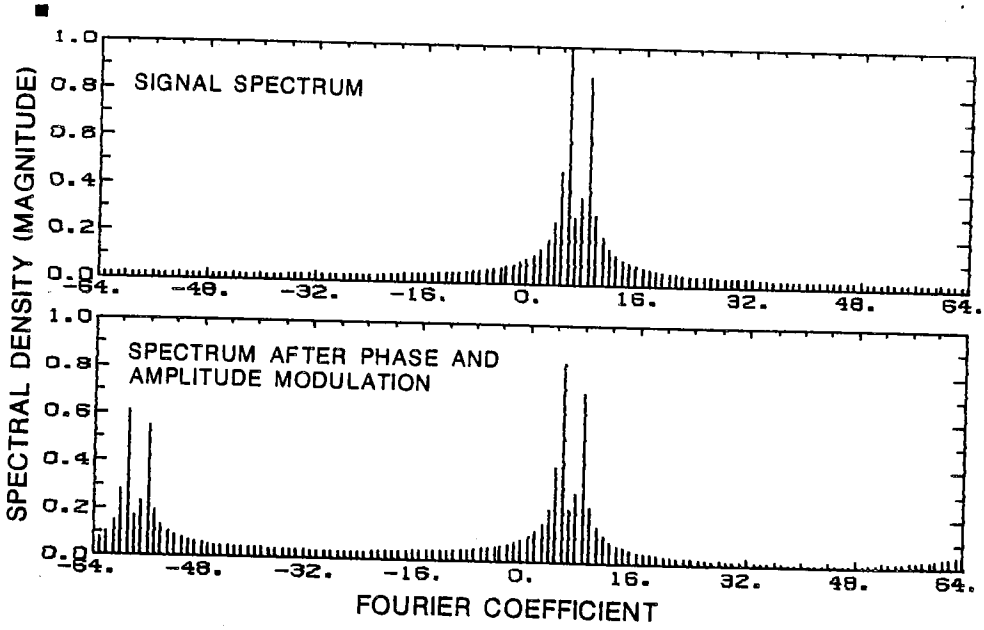

Figure 5. Spectra of a signal before and after phase and amplitude modulation.

We see that the spectrum has two peaks separated by the Nyquist velocity and the two halves of the spectrum (at positive and negative velocities) are remarkably similar in shape, except for an amplitude difference. The radar cross section of the hydrometeor scatterers is different for the two polarizations thus, the amplitude modulation of the signal. Clearly the polarization switching has modulated the echo signal and altered the signal spectrum. In order to recover the mean velocity we should know the nature of the spectrum before modulation. Similarly, the total propagation phase shift of the signal from the radar antenna to the resolution volume and back to the radar is also different for the two polarizations giving rise to a phase modulation of the signal. To understand the effect of modulation on the spectral shape, let us modulate, in phase and amplitude, a narrow band signal, and examine the resulting spectrum. Let $V(iT_s)$ be complex voltage samples of a signal without modulation at time (iT_s) and $a(k)$ be the k^{th} complex Fourier coefficient obtained by a DFT operation. Then, using the inverse DFT operation, we can write:

$$V(iT_s) = \frac{1}{M} \sum_{k=0}^{M-1} a(k) e^{j2\pi ik/M} \tag{13}$$

Because the spectrum is narrow compared to the Nyquist interval, the coefficients $a(k)$ are non-zero only in a narrow region centered around $k=k_1$ corresponding to the mean Doppler frequency of the signal. Let $e^{z(-1)^i}$ be the modulation sequence where the real part of the complex exponent $z = (\alpha + j\beta)$ represents amplitude modulation and the imaginary part the phase modulation. Thus $40\alpha\log(e)$ is the expected value of differential reflectivity and 2β the expected value of differential phase. The spectral coefficients of the modulated sequence $s(k)$ are represented as:

$$s(k) = \sum_{i=1}^{M} V(iT_s) e^{z(-1)^i} e^{-j2\pi ik/M} \tag{14}$$

Substituting (13) in (14) we have

$$s(k) = \sum_{i=1}^{M} \sum_{\ell=0}^{M-1} a(\ell) e^{j2\pi i(\ell-k)/M} e^{z(-1)^{\frac{i}{2}}} \tag{15}$$

which can be reduced to

$$s(k) = a(k)\cosh(z) + a(k+\tfrac{M}{2}) \sinh(z) \tag{16}$$

Similarly the spectral coefficient $s(k+\frac{M}{2})$ is:

$$s(k+\tfrac{M}{2}) = a(k)\sinh(z) + a(k+\tfrac{M}{2})\cosh(z). \tag{17}$$

Because of our assumption of a narrow spectrum, either a(k) or $a(k + \frac{M}{2})$ would be zero, (this condition may not be exactly satisfied in the actual radar signal because of the noise and the window effect, but would be nearly satisfied in most cases) but after modulation the spectral coefficients s(k) and $s(k + \frac{M}{2})$ would have significant magnitudes. In fact, the power in the coefficient a(k) of the original spectrum is divided between the two coefficients s(k) and $s(k + \frac{M}{2})$ of the modified spectrum. Thus, a replica of the original spectrum shape appears in the modified spectrum and is centered at $(k_1 + \frac{M}{2})$ corresponding to a mean velocity $v \pm v_a$. Figure 5 shows graphically the effect of modulation. It can be shown that when amplitude modulation is present and there is no phase modulation the complex spectral coefficients of the modulated signals s(k) and s(k + M/2) will have the same phase. With phase only modulation the phase difference between s(k) and s(k + M/2) will be 90°, the amount of phase modulation determines the relative magnitudes of these two spectral coefficients.

If we use spectral processing (Zrnic, 1979) to recover the mean radial velocity and the spectrum width we would get a velocity equal to v or $v \pm v_a$, but the width can be recovered if a provison is made to recognize the two distinct

spectra. In figure 6 we have shown typical spectra of H and V samples taken separately. Note that because there are only half the number of samples in each of the sample sequences the PRT is twice that for the combined signal and, the Nyquist interval is also halved in spectra. The remarkable similarity of the shape of H and V spectra indicates that the two sequences have a very high correlation. The same shape is nearly reproduced in the combined spectra (see Fig. 4) hence, it is possible to estimate the mean velocity and spectrum width using only half the spectrum, but with an ambiguity in the estimated mean velocity. Additional information is needed to resolve this ambiguity.

In an ideal case, where the modulation function z (see eq. 14) is a constant, one can determine z and hence the original sample series $V(iT_s)$ can be recovered. The recovery of z seems simple from equations (16) and (17) in which a(k) or $a(k + \frac{M}{2})$ is assumed to be zero. However, because of noise and the window effect, both a(k) and $a(k + \frac{M}{2})$ are non-zero. Thus, to recover z a more elaborate analysis is required. The problem is further complicated by statistical perturbations present in the modulation function z. Figure 7 shows some typical spectra with low SNR, from which it is clear that recovery of z from a pair of spectral coefficients separated by M/2 coefficients is not always possible.

Because of the large computation required in the case of spectral processing, most radars use the simpler autocovariance processing (pulse pair) for mean velocity and spectrum width estimation. Equation (4) uses only the phase of the autocorrelation estimate in calculating the velocity, whereas, the spectrum width calculation uses the magnitude information (eq. 6). We shall see how the polarization switching affects the autocorrelation.

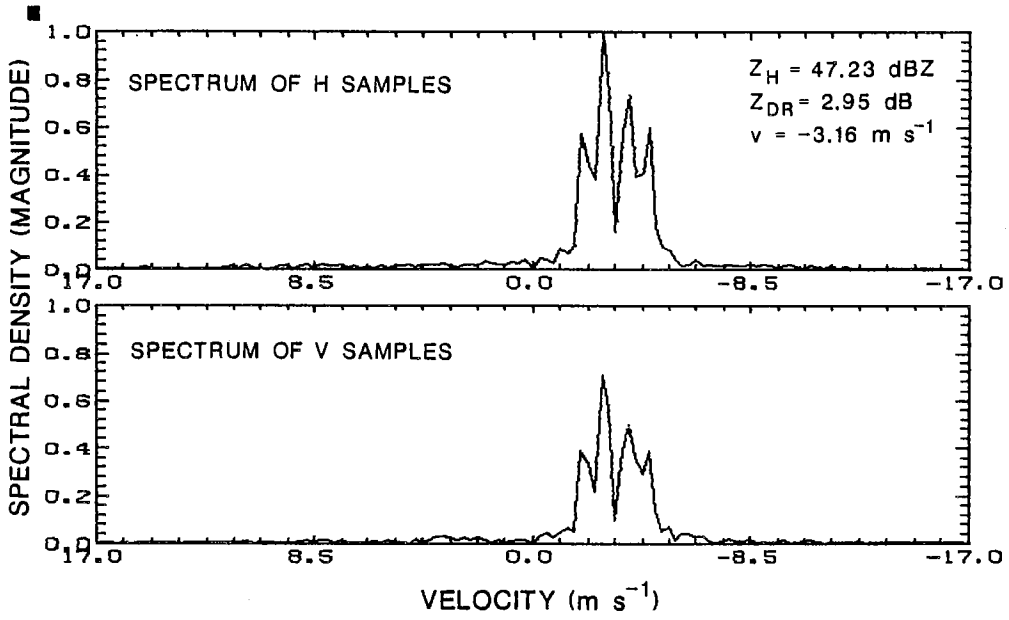

Figure 6. Spectra of separated H and V samples for the same data as in fig. 4.

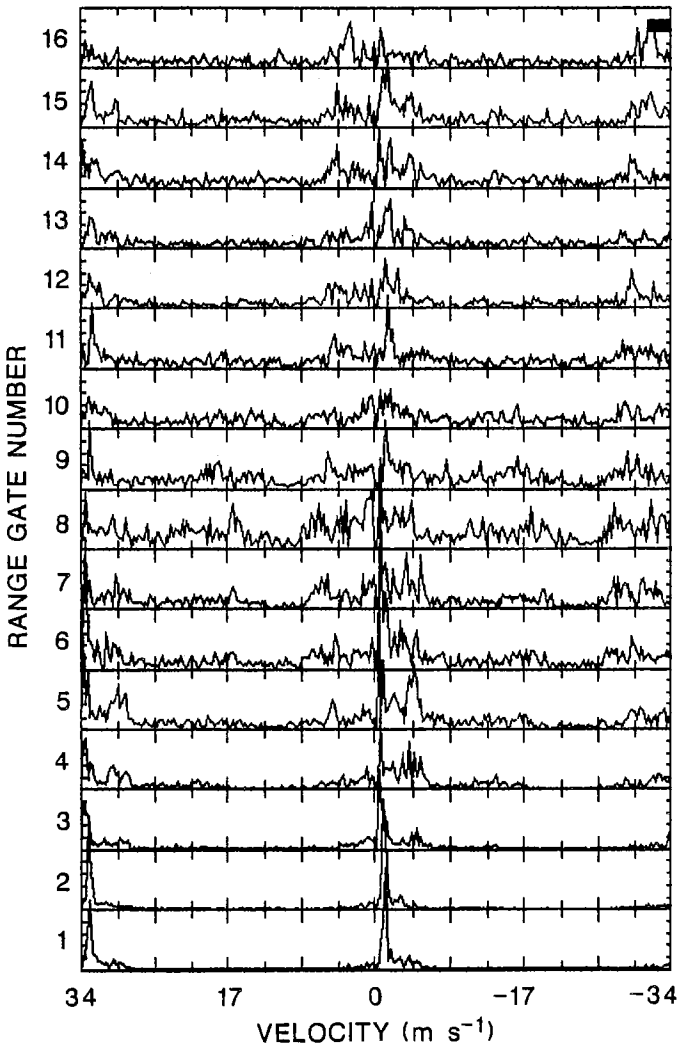

Figure 7. Spectrum of the dual polarized radar signal with low SNR.

With alternate polarization switching, the autocorrelation estimate using the conventional (pulse pair) processor can be expressed as:

$$\hat{R}(T_s) = \frac{1}{M} \sum_{i=1}^{M/2} \left(H^*_{2i} V_{2i+1} + V^*_{2i+1} H_{2i+2}\right) \tag{18}$$

Summing the two products in (18) separately and representing them by $\hat{R}_a$ and $\hat{R}_b$ we have

$$\hat{R}_a(T_s) = \frac{2}{M} \sum_{i=1}^{M/2} H^*_{2i} V_{2i+1} \tag{19}$$

$$\hat{R}_b(T_s) = \frac{2}{M} \sum_{i=1}^{M/2} V^*_{2i+1} H_{2i+2} \tag{20}$$

and $$\hat{R}(T_s) = \frac{1}{2} [\hat{R}_a + \hat{R}_b] \tag{21}$$

True values of estimates $\hat{R}_a$ and $\hat{R}_b$ are the expected values of products $H^*_n V_{n+1}$ and $V^*_n H_{n+1}$ respectively. Using equation (1) we can write R_a as:

$$R_a = \langle H^*_n V_{n+1} \rangle$$

$$= K^2 \sum_i \sum_\ell \langle s^{*i}_h s^\ell_v I^{*i} I^\ell \rangle \langle \exp\{j[\gamma^i_h(n) - \gamma^\ell_v(n+1)]\} \rangle \tag{22}$$

Because the resolution volume dimensions are large compared to the wavelength, $\gamma^i_{h,v}(n)$ are uniformly distributed over $(0\text{-}2\pi)$. Hence, the expectation of the exponential in (22) is zero except when $i=\ell$, reducing the double summation to a single summation.

$$R_a = K^2 \sum_i \langle s^{*i}_h s^i_v \rangle |I_i|^2 \langle \exp\{j[2(k_h-k_v)r_{n,i} - 2(k_o+k_v)T_s v_i]\} \rangle \tag{23}$$

The term $2(k_h-k_v)r_{n,i}$ has a narrow distribution about $2(k_h-k_v)r_o$, where r_o is the range to the center of resolution volume, and the term $2T_s(k_o+k_v)v_i$ has a narrow

distribution about $2T_s(k_o+k_v)v$, where v is the mean velocity. Thus, the expected value of the exponential reduces (23) to:

$$R_a = K^2 \sum_i \langle s_h^{*i} s_v^i \rangle \, |I_i^2| \, \exp\{j[2T_s(k_o+k_v)v + 2(k_h - k_v)r_o]\} \tag{24}$$

Similarly we can derive R_b as

$$R_b = K^2 \sum_i \langle s^*{}_v{}^i s_h{}^i \rangle \, |I_i|^2 \, \exp\{j[2T_s(k_o+ k_h)v-2(k_h- k_v)r_o]\} \tag{25}$$

It is evident from (24) and (25) that the phase of R_a is the sum of phases due to the Doppler shift, $\psi_d = 2T_s(k_o + k_h)v$, and the two way differential propagation phase shift, $\phi_{DP} = 2(k_h - k_v)r_o$, whereas the phase of R_b is the Doppler phase, ψ_d, minus the ϕ_{DP}. Thus, we can write the expected (or true) $R(T_s)$ as:

$$R(T_s) = \frac{1}{2}\left[|R_a| e^{j(\psi_d + \phi_{DP})} + |R_b| e^{j(\psi_d - \phi_{DP})} \right] \tag{26}$$

The magnitudes of R_a and R_b are equal, and we can simplify (26) to:

$$R(T_s) = |R_a| \cos(\phi_{DP}) e^{j\psi_d} \tag{27}$$

This equation holds approximately for the estimates as well. Thus, we can estimate the Doppler phase shift ψ_d using the conventional autocovariance processor only when ϕ_{DP} is less than 90°. When ϕ_{DP} approaches 90°, we see that the magnitude of $R(T_s)$ tends to zero, hence, the recovered mean velocity would be very noisy around $\phi_{DP} = 90°$. When ϕ_{DP} is greater than 90° it is easy to see from (27) that the estimated velocity would be off by v_a (i.e., ψ_d is shifted by 180°, making, for example, a small positive velocity appear as large negative velocity). However, this ambiguity can be resolved if ϕ_{DP} is also estimated. From the theory, we know that ϕ_{DP} is always positive for the rain medium because rain drops are oblate with their axis of rotational symmetry aligned along the vertical and

most of the propagation phase shift is in the rain medium. On the other hand if hydrometeors are primarily composed of ice the differential phase shift is expected to be small ($|\phi_{DP}| << 90°$). In figure 8.a we show conventionally processed pulse pair velocity estimates along a radial. The corresponding integrator output record and the spectrum width estimates from the pulse pair processor are shown in figures 8.b and 8.c. Note the nearly constant but large spectrum width estimates (fig. 8.c) from the conventional pulse pair estimator due to the modulation discussed earlier. The noisy velocities in the figure 8.a for ranges less than 30 km and greater than 80 km are due to the low SNR as can be inferred from the integrator output (fig. 8.b) which is proportional to the received echo power. A discontinuity in the velocity around 45 km range is attributed to the differential propagation phase shift. Note also the noisy region around the point of discontinuity where the SNR is not small. From our analysis we can infer that the differential propagation phase shift is around 90° in the region of discontinuity. This is clearly shown in the figure 8.d, in which we have plotted: 1) the conventional pulse pair velocity estimate (eqn. 4), 2) the velocity derived from a modified estimator (eq. 30 - discussed later in this section) and 3) the corresponding differential propagation phase shift $\hat{\phi}_{DP}$, along a radial; all parameters have been calculated from the time series records. Note that the conventional pulse pair estimator and the modified estimator give the same velocity value as long as $\hat{\phi}_{DP}$ is less than 90°; when $\hat{\phi}_{DP} \approx 90°$ conventional pulse pair estimates become noisy and for $\hat{\phi}_{DP} > 90°$, the velocity shifts by v_a, the Nyquist velocity.

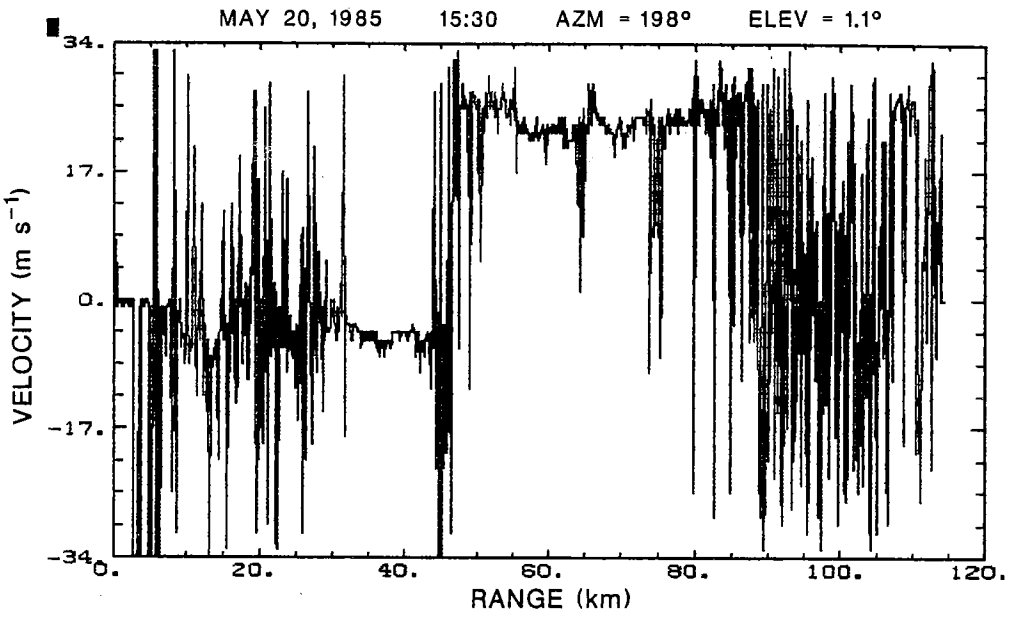

Figure 8(a). Velocity estimates along a radial obtained by a hard wired conventional pulse pair processor.

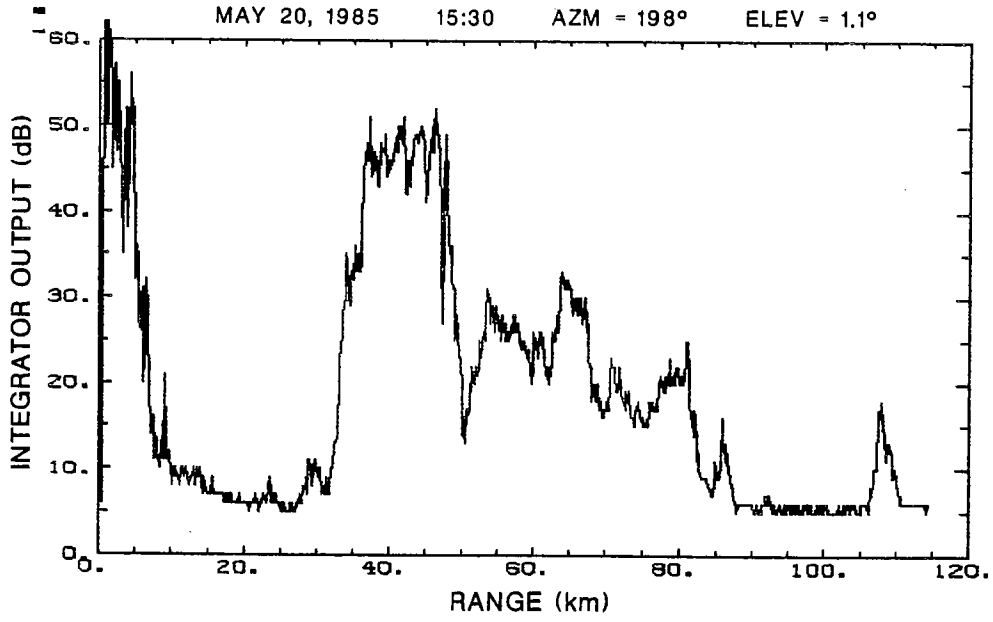

Figure 8(b). Integrator output record corresponding to the radial in figure 8.a.

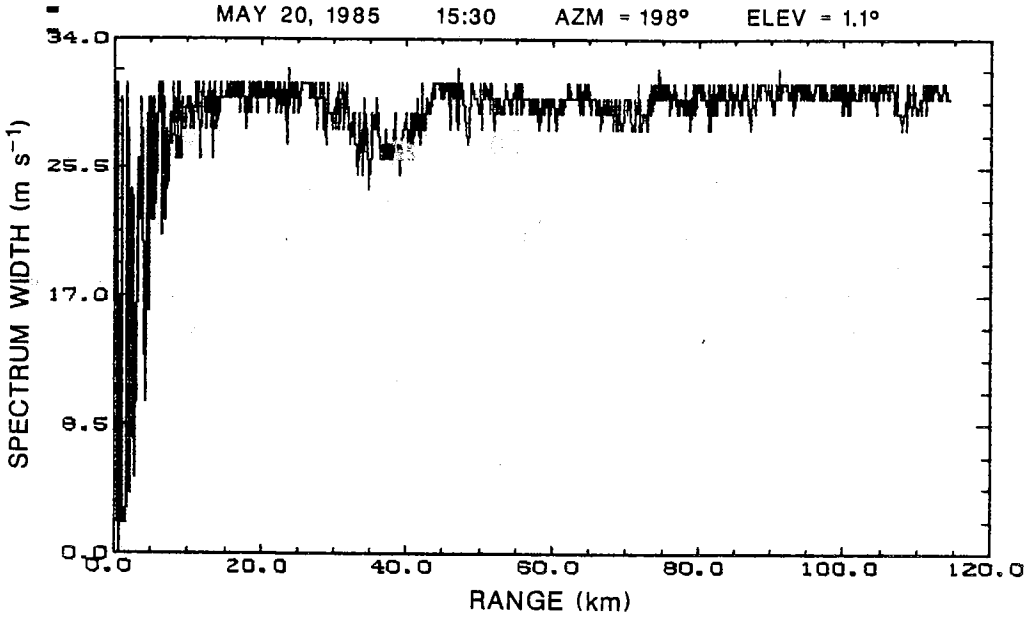

Figure 8(c). Spectrum width record from the conventional pulse pair processor, for the same radial as in fig. 8.a.

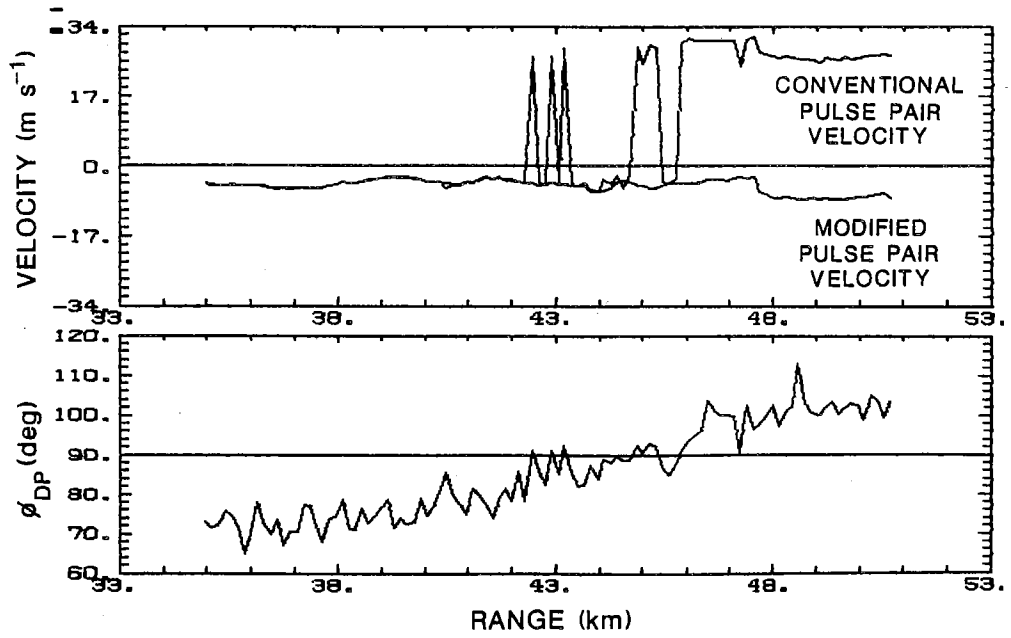

Figure 8(d). A comparison of velocity estimates from the conventional pulse pair estimator (4) and the modified estimator (30). The corresponding ϕ_{DP} estimates are also shown.

The modified estimator is able to extract correct velocity for the complete range interval. It not only removes the noisy band in the velocity estimate but also enables us to resolve the velocity ambiguity. The estimator requires separate calculation of R_a and R_b and determinion of ϕ_{DP}. A suggested estimator for ϕ_{DP} is (Sachidananda and Zrnić, 1986):

$$\hat{\phi}_{DP} = \frac{1}{2} \arg(\hat{R}_a \hat{R}_b^*) \tag{28}$$

The number of sample pairs required to achieve a 1° standard error in $\hat{\phi}_{DP}$ using (28) is approximately 30 to 40 (Sachidananda and Zrnić, 1986). Figure 9 gives the standard error performance of the estimator versus the number of sample pairs averaged to determine $\hat{R}_a$ and $\hat{R}_b$.

It appears that (28) gives ambiguous $\hat{\phi}_{DP}$ when the actual value is outside a 180° interval, but it is easy to resolve this ambiguity knowing the information that ϕ_{DP} is always positive in the rain medium and is a monotonically increasing function of the range. If the differential phase shift in the radar system is adjusted to zero, ϕ_{DP} would have a value 0° for a clear path and starts increasing only when the propagation path encounters precipitation. Thus, it is tempting to locate the unambiguous 180° interval from 0° to 180° and use continuity of ϕ_{DP} in range to correct the ambiguity whenever two consecutive values differ by a large amount (e.g. more than 90°). But at close range when ϕ_{DP} is small statistical uncertainty may produce small negative values and these mustn't be changed. This suggests that range dependent correction procedure should be used on ϕ_{DP} data.

An estimator similar to (28) for mean velocity estimation could be:

$$\hat{v} = -\frac{v_a}{2\pi} \arg(\hat{R}_a \hat{R}_b) \tag{29}$$

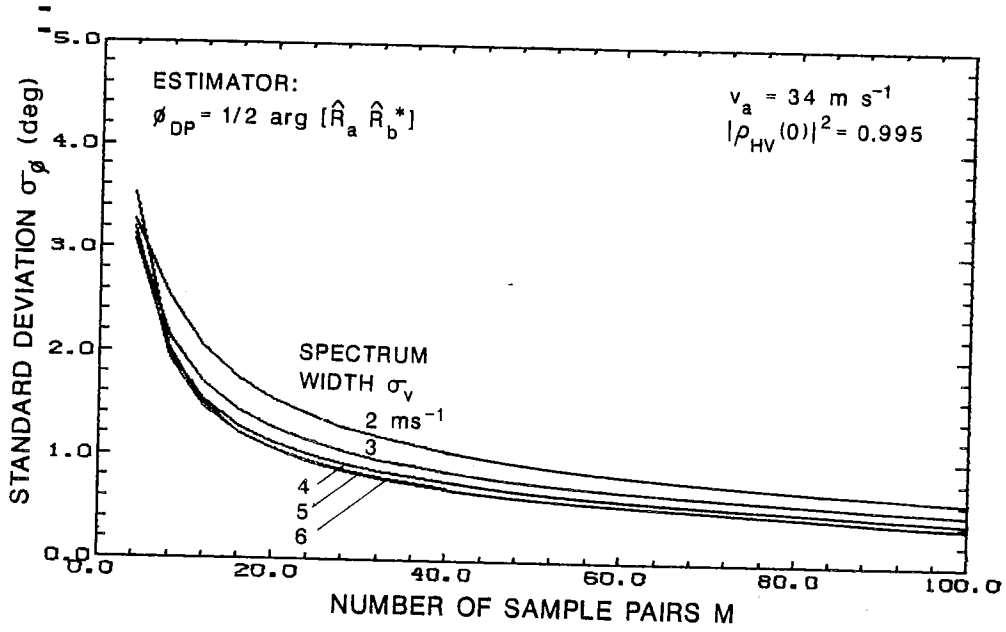

Figure 9. Standard error in ϕ_{DP} estimates. $\rho_{HV}(0)$ is the correlation coefficient between horizontally and vertically polarized echoes at lag 0.

Here, it is not easy to resolve the ambiguity because the actual velocity can be in the interval $\pm v_a$ (when there is no velocity aliasing) but (29) gives velocity values within $\pm v_a/2$. Since, we have already determined $\hat{\phi}_{DP}$, velocity can be recovered unambiguously using:

$$\hat{v} = -\frac{v_a}{\pi}\left[\arg\left(\hat{R}_a\right) - \hat{\phi}_{DP}\right] \qquad (30)$$

where $\hat{\phi}_{DP}$ is a positive (corrected value).

Although the number of pulse pair products averaged in $\hat{R}_a$ and $\hat{R}_b$ are half that would be available in the case of a single polarized radar, the variance of the estimates is nearly the same because for a sufficiently large M the variance is mainly a function of the decorrelation time and the total sampling period, which are the same in both cases [(for var($\hat{v}$) see Zrnić, 1979].

In figures (10.a) through (10.d) we show some plots of consecutive complex product vectors $(H_i^* V_{i+1})$ and $(V_{i+1}^* H_{i+2})$, for a few time series records. Each point corresponds to the tip of a product vector and the axis are in arbitrary units. The figures clearly indicate that the product vectors form two distinct groups. In fact, all the vectors in the upper half are (H^*V) products and the ones in the lower half are (V^*H) products; the mean of these two groups represent $\hat{R}_a$ and $\hat{R}_b$ respectively. The remarkable similarity in the pattern of distribution of the component vectors of $\hat{R}_a$ and $\hat{R}_b$ is due to the high correlation between H and V samples ($|\rho_{HV}(0)|^2 \approx 0.995$). The inference from (27) that the mean velocity estimate would be noisy when ϕ_{DP} is near 90°, is obvious from these figures. When $\phi_{DP} = 90°$ the two mean vectors $\hat{R}_a$ and $\hat{R}_b$ would exactly oppose each other making the sum of the vectors nearly zero. The angular spread of the component vectors in each group is a measure of the spectrum width of the signal.

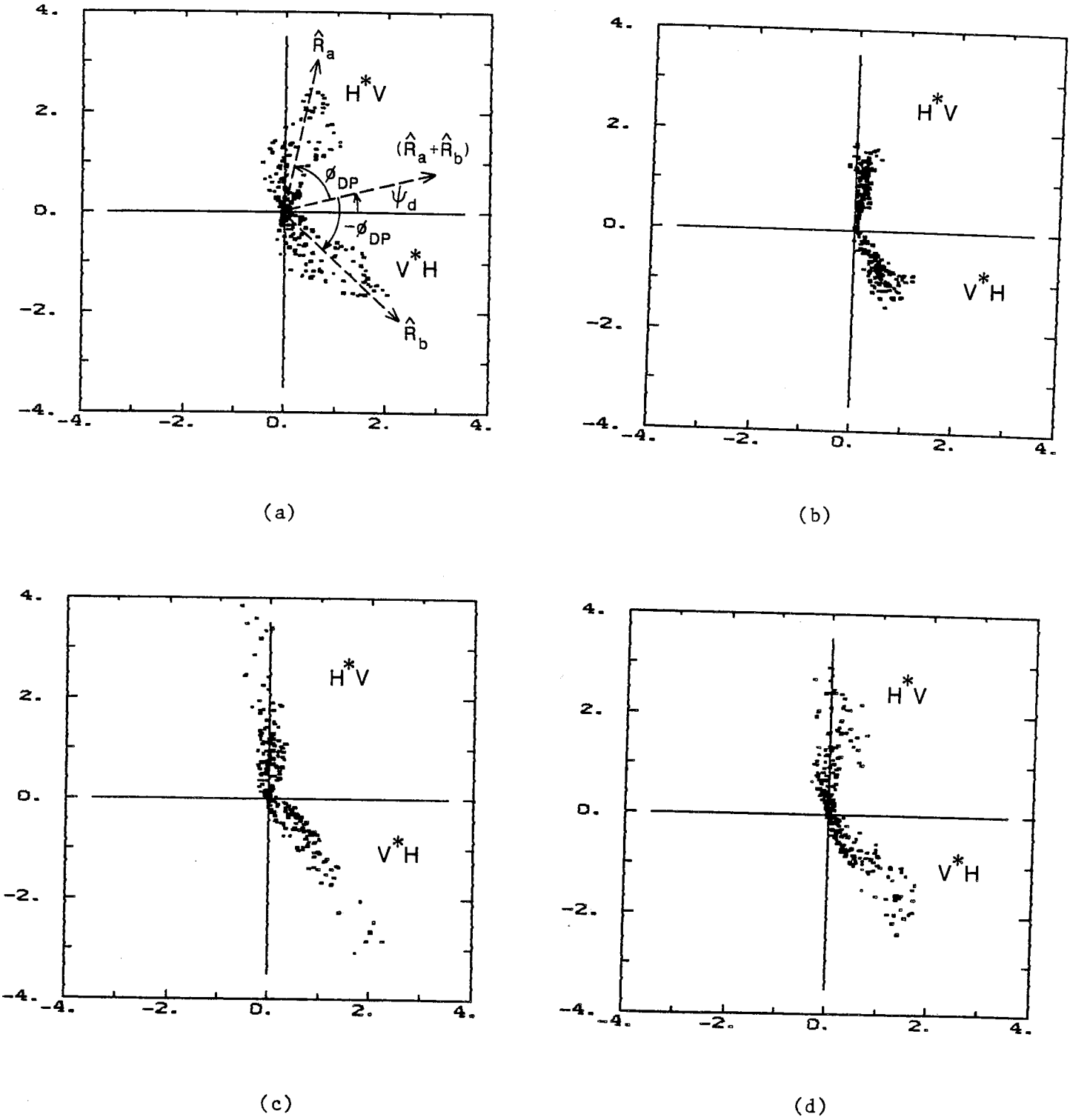

Figure 10. Complex pulse pair product vectors from a time series record. x,y axes are in arbitrary units.

3.3. Spectrum Width:

Weather signals normally have Gaussian power spectra for which the correlation coefficient for m pulse lag, $\rho(mT_s)$ is (Zrnić 1977):

$$\rho(mT_s) = \exp(-8\pi^2\sigma_v^2 T_s^2 m^2/\lambda^2)\ \exp(-j2\pi f_d T_s m) + \delta_m \cdot SNR^{-1} \qquad (31)$$

where σ_v is the spectrum width in (ms^{-1}) and f_d is the mean Doppler frequency.

In a radar with alternating polarization, samples of equal polarization are available only at a PRT of $2T_s$, thus, $\rho(mT_s)$ can be calculated for even values of m. The spectrum width σ_v can be estimated with an estimator which uses $\hat{R}(2T_s)$ (see Zrnić 1979), but additional computation is required to estimate $R(2T_s)$. Further, the estimator using $\hat{R}(2T_s)$ does not perform as well, compared to the estimator using $\hat{R}(T_s)$. It would be preferable, computationally and accuracy-wise, to estimate σ_v from $\hat{R}_a(T_s)$ which is readily available from the pulse pair velocity processor.

We can express the autocorrelation R_a as

$$R_a(T_s) = \langle H_i^* V_{i+1} \rangle = (S_H S_V)^{1/2}\, r_{HV}(T_s) \qquad (32)$$

where $S_{H,V}$ are the mean sample powers of H and V samples respectively and r_{HV} is the correlation coefficient for H and V pair. The samples H_i and V_{i+m} decorrelate mainly due to (a) the Doppler spread and (b) the drop shape and canting angle distribution (Sachidananda and Zrnić, 1985). Because these two processes can be assumed to be statistically independent, we can write:

$$R_a(T_s) = (S_H S_V)^{1/2}\, \rho(T_s)\ \rho_{HV}(T_s) \qquad (33)$$

where $\rho(T_s)$ is the correlation coefficient due to the Doppler spread, and $\rho_{HV}(T_s)$ is the correlation coefficient arising from drop shape and canting angle

distribution. We can approximate $\rho_{HV}(T_s) \approx \rho_{HV}(0)$ because the changes in the distribution of drop shape and canting angle are small over the sampling time, thus, can be assumed to be independent of time. In most cases $|\rho_{HV}(0)|$ is nearly unity (>0.997) hence, the spectrum width can be estimated from the formula:

$$\hat{\sigma}_v = \frac{\sqrt{2}v_a}{\pi} \left| \ell n \left[\frac{\hat{S}_H \hat{S}_V}{|\hat{R}_a \hat{R}_b|} \right]^{1/2} \right| \operatorname{sgn}\left[\ell n \left[\frac{\hat{S}_H \hat{S}_V}{|\hat{R}_a \hat{R}_b|} \right]^{1/2} \right] \qquad (34)$$

Note that (34) is derived from the conventional spectrum width estimator by replacing $\hat{R}$ by $|\hat{R}_a \hat{R}_b|^{1/2}$ and $\hat{S}$ by $(\hat{S}_H \hat{S}_V)^{1/2}$. For a sufficiently large M, $|\hat{R}_a|$ and $|\hat{R}_b|$ are identical thus, the performance of this estimator would be nearly the same as the conventional one.

3.4 A signal processing scheme for echoes with alternating polarization

Figure 11 is a signal processing schematic for a radar with alternating polarization; it incorporates all the modifications suggested in previous sections. The $\hat{Z}_{DR}$ is derived using a square law estimator which has much lower standard error than a logarithmic estimator. The reflectivity is also derived from I and Q samples. Note the additional accumulator in the reflectivity processor and in the pulse pair processor, to store the values for the two polarizations separately. The calculation procedure for the mean velocity and the spectrum width should proceed as in (30) and (34).

4. Analysis of radar signals and some observations

In this section, we discuss several considerations that require attention in order to correctly interpret echo properties. Prominent among these are sidelobe contamination, sample correlation, spectral shape etc. which can affect accuracy of scatter matrix estimation. For the most part, we have compiled a large number of figures derived from data in one sector sweep. A number of observations have

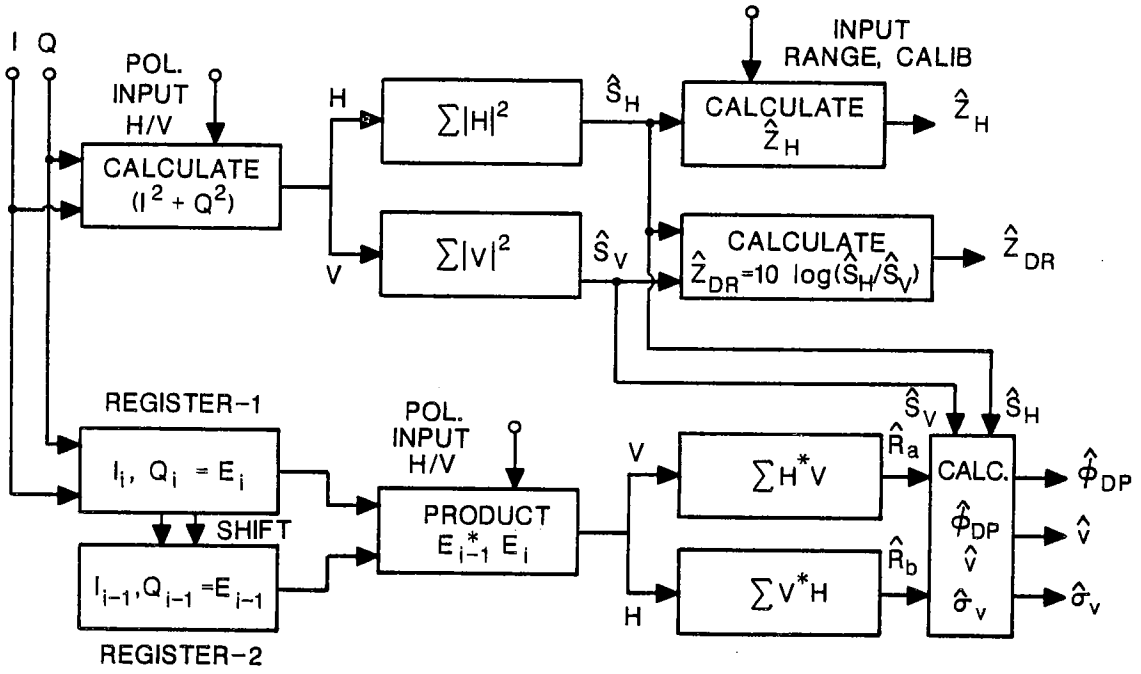

Figure 11. A signal processing scheme for a radar with alternating polarization.

been made with some discussion on the possible interpretations, but these are mostly inconclusive. In many cases further work is needed to arrive at any definite conclusions. So, the reader may find this section somewhat disconnected, sometimes speculative, and touching upon several observations. However, we hope that the observations made herein provide enough food for thought and would aid in identifying areas for further investigation.

4.1. Side lobe contamination:

It is generally an accepted practice to estimate the radar observables from the received signal samples and assign them to the radar resolution volume. But, this is strictly valid only when an antenna pattern is an ideal sector beam of finite width with no side lobes and the range weighting function is similarly limited. In this section we shall confine our attention only to the antenna. A concise discussion of side lobe effects on multiparameter radar measurements was performed by Johnson (1984).

Practical antennas have side lobes spread over a large solid angle compared to the narrow main beam; and considering the large dynamic range of weather signals ($\approx$ 80 dB) and the large spatial extent of the distribution of scatterers, the power received through the antenna side lobes can be a significant fraction of or even larger than the echo power received through the main lobe. To get an idea of the order of magnitude of the side lobe power relative to the main lobe power, let us take, for example, a hypothetical antenna power pattern with 1° main beam width and a uniform -30 dB side lobe spread over an angular sector $\pm 15°$ in both horizontal and vertical planes. Though the pattern shape is unrealistic, the magnitude of angles and side lobe levels approximately corresponds to that found in a practical weather radar antenna; perhaps a little on the conservative side. If the $\pm 15°$ angular sector containing mainbeam and side lobes is completely

covered by scatterers with uniform reflectivity, we would get a main lobe to side lobe signal power ratio, p_{ms} = 30.5 db. This implies that the main lobe signal and the side lobe signal would have equal powers (p_{ms} = 0 dB) when the main beam is pointing in a direction of reflectivity factor 30.5 dBZ lower than the mean reflectivity factor of the ±15° sector.

Now, let us suppose that the antenna is pointing nearly in a horizontal direction (low elevation) and the range gate is at 50 km. Further, if we assume a rain filled region approximately to a height of 2 km from the ground, the vertical angular coverage of the scatterers is approximately 2-3°, much less than the ±15° sector of the side lobes. Thus, p_{ms} would be approximately equal to 41.5 dB. At shorter ranges the regular sector in the vertical direction increases, hence, p_{ms} would be lower. It may be noted that in practice the angular sector of the storm as well as the antenna side lobes can be much larger, resulting in lower p_{ms} values.

With a p_{ms} of 10 dB the reflectivity factor would be overestimated by about 0.4 dBZ which is much less than the 1 dB standard error of most reflectivity estimates in practical radars. It appears that reflectivity is not very seriously affected by the side lobes; at least in the high reflectivity region of the storm.

The effect of side lobes on the Z_{DR} estimate is more serious than that on reflectivity Z_H. Although the main lobes of the antenna patterns for the horizontal and the vertical polarizations can be made to match reasonably well, it is very difficult to match the side lobes, and matching the side lobes would not be of much help either. If the main lobe and side lobes are matched for the two polarizations, the scatterers illuminated by side lobes must have the same Z_{DR} as that of the scatterers illuminated by the mainbeam, in order that the estimated Z_{DR} is error free. Otherwise there would be some bias error depending on the

difference in the Z_{DR} values of scatterers in the main beam and side lobes and their relative powers. When the side lobes are not matched, the side lobe powers in the vertical and the horizontal polarizations differ not only because of the Z_{DR} of the scatterers, but also due to the different antenna pattern weighting in each polarization. In the presence of side lobe signal, we can represent the Z_{DR} estimate as:

$$\hat{Z}_{DR} = 10 \log \left[\frac{\hat{P}_{Hm} + \hat{P}_{Hs}}{\hat{P}_{Vm} + \hat{P}_{Vs}}\right] \tag{35}$$

where supscripts H,V represent polarizations and m,s represent the main lobe and side lobes respectively. It is clear from (35) that the Z_{DR} estimate would not be affected if the main lobe to side lobe signal power ratio, p_{ms}, is the same for both polarizations. It is simple to see that the difference in the over-estimate of Z_H and Z_V (in dBZ), due to the side lobe signal, appears as the error in Z_{DR} estimate. Thus, if Z_H is over-estimated by 0.4 dB (p_{ms} = 10 dB) and Z_V is over-estimated by 0.2 dB (p_{ms} = 13 dB), Z_{DR} would be in error by +0.2 dB.

It may be noted that the side lobe signal always contributes to overestimates of Z_H and Z_V, while the error in Z_{DR} can be positive or negative. It is reasonable to assume that the spatial distribution of the error due to side lobe signal is random thus one can reduce the side lobe bias error in Z_{DR} by spatial averaging. In general, for a storm with 55 dBZ peak reflectivity core one can expect a side lobe bias error in Z_{DR} in the order of 0.2 dB or more at the edges of the storm with reflectivities less than about 25 dBZ, if no averaging is employed.

The effect of side lobe contamination on the phase of the signal is much more severe than that on Z_H and Z_{DR}, which are functions of the sample power. Thus the differential propagation phase shift is much more susceptible to side lobe contamination. The following analysis provides some idea about the order of magnitude of the error in phase estimation due to the side lobe signal.

Because different scatterers contribute to the main lobe and side lobe signals, we can assume them to be statistically independent. Thus, we can write autocorrelation as a sum of autocorrelations for the main lobe signal and the side lobe signal. Thus, the autocorrelations $\hat{R}_a$ and $\hat{R}_b$ (see eqns. 19, 20) can be written as:

$$\hat{R}_a(T_s) = \frac{2}{M} \sum_{i=1}^{M/2} H_{2i}^* V_{2i+1}$$

$$= \hat{R}_{am} + \hat{R}_{as} \tag{36}$$

and $$\hat{R}_b(T_s) = \frac{2}{M} \sum_{i=1}^{M/2} V_{2i+1}^* H_{2i+2}$$

$$= \hat{R}_{bm} + \hat{R}_{bs} \tag{37}$$

where the subscripts m,s refer to the main lobe and side lobe respectively. Note that the two autocorrelations $\hat{R}_{am}$, $\hat{R}_{as}$ add vectorially. Thus, the phase error due to the presence of the side lobe signal is maximum when the two autocorrelations are orthogonal to each other, assuming the side lobe signal to be smaller than the main lobe signal. Let us examine the expected (or true) value of the product $\hat{R}_a \hat{R}_b^*$, and its argument from which $\hat{\phi}_{DP}$ is obtained.

$$R_a R_b^* = \left[|R_{am}| \, e^{j(\phi'_{DP} - \psi'_d)} + |R_{as}| e^{j(\phi''_{DP} - \psi''_d)} \right]$$

$$\times \left[|R_{bm}| \, e^{j(\phi'_{DP} + \psi'_d)} + |R_{bs}| e^{j(\phi''_{DP} + \psi''_d)} \right] \tag{38}$$

In (38) single prime (') represents the phase of the main lobe signal and double prime (") represents the phase of the side lobe signal. Dividing (38) by $|R_{am}||R_{bm}|$ and simplifying we have:

$$\frac{R_a R_b^*}{|R_{am}|\,|R_{bm}|} = e^{j2\phi'_{DP}} + p_{ms}^{-2} e^{j2\phi''_{DP}} + p_{ms}^{-1}\, 2\cos(\psi'_d - \psi''_d)\, e^{j(\phi'_{DP} + \phi''_{DP})} \qquad (39)$$

where p_{ms} is the main lobe to side lobe signal power ratio. Further, we have made use of the identities $|R_{am}| = |R_{bm}|$, $[R_{as}| = |R_{bs}|$ and $p_{ms} = |R_{am}|/|R_{as}|$. For p_{ms} sufficiently large we can neglect the second term in (39); the last term is the major contributor to the phase error. In the worst case, when the cosine term is unity and the first and the third terms are in phase quadrature, the phase error in ϕ_{DP} would be equal to $0.5\ \tan^{-1}(p_{ms}^{-1})$.

If ϕ_{DP} is to be useful in rainfall rate estimation, we need an accuracy of about 0.5° in the estimate. To guarantee this accuracy p_{ms} has to be 18 dB. This limit is very difficult to achieve in practice, except in regions of uniform reflectivity or with exceptionally good antennas.

The relative estimation accuracy required of the mean velocity is an order of magnitude less; approximately 1 m s^{-1} in the unambiguous interval of 68 m s^{-1} would be acceptable in most cases. Although mean velocity estimator (30) uses only $\hat{R}_a$, a simple calculation shows that the maximum phase error in the case of velocity estimation is approximately equal to $\tan^{-1}(p_{ms}^{-1})$. For an unambiguous velocity v_a = 34 ms^{-1} and a maximum side lobe bias error of 1 m s^{-1}, the tolerable phase error is 5.3° which can be achieved if p_{ms} is larger than about 10 dB.

Figures 12.a to 12.d show some examples of side lobe contamination in the estimated differential propagation phase shift ϕ_{DP}. Each figure is a plot of Z_H, Z_{DR}, and ϕ_{DP} along a radial sampled at intervals of 150 m. From the statistics of ϕ_{DP} estimator (Fig. 9) we expect that, for 128 sample pairs used in estimating all three parameters, theoretically predicted standard error should be less than 0.5°. Further, ϕ_{DP} is a monotonically increasing function of the range because it

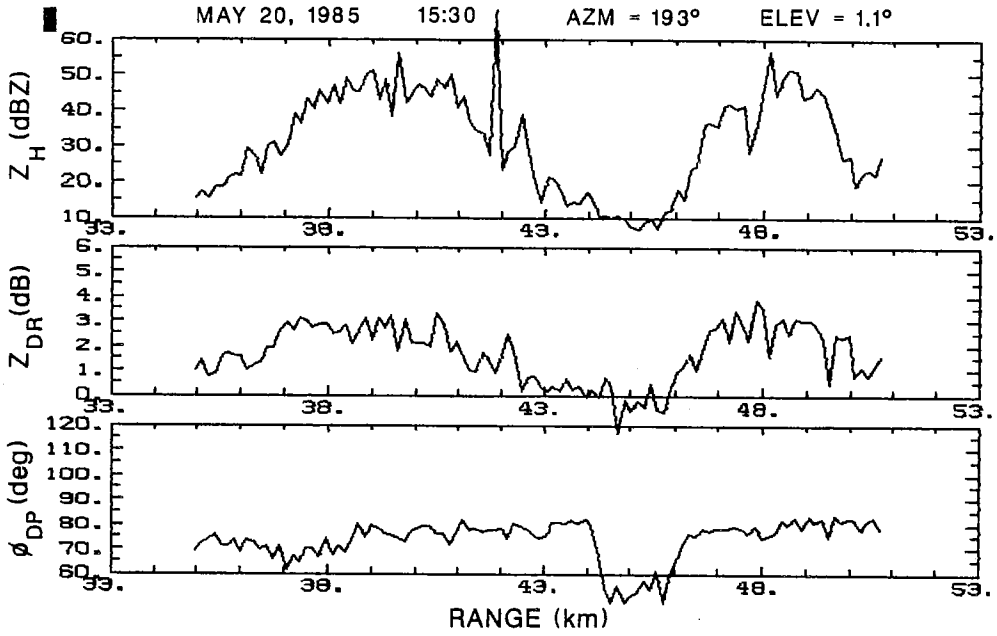

(a)

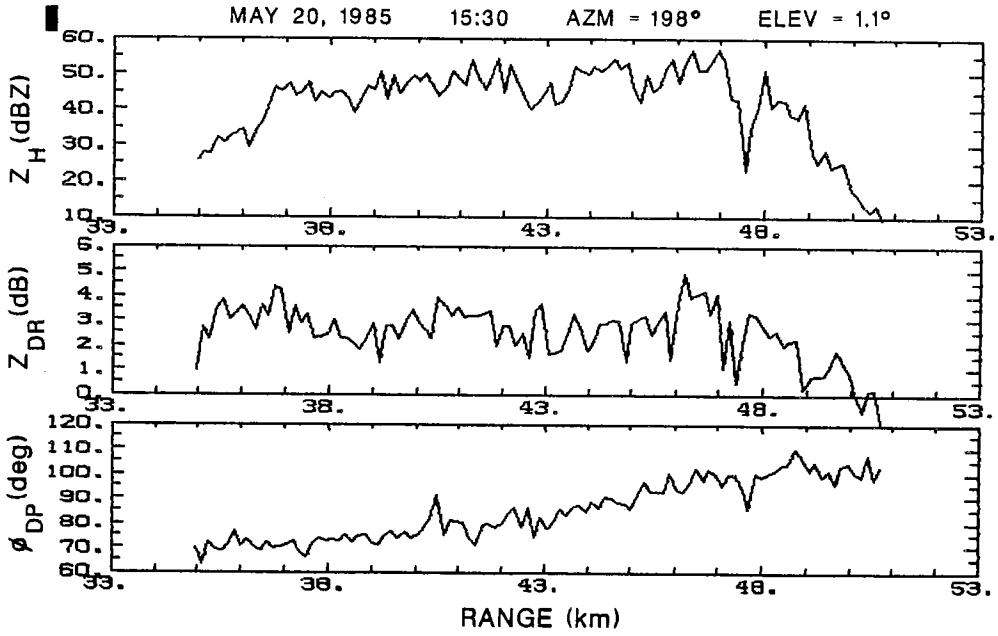

(b)

Figure 12. Estimated Z_H, Z_{DR} and ϕ_{DP} along a radial. Number of sample pairs for the estimates is 128.

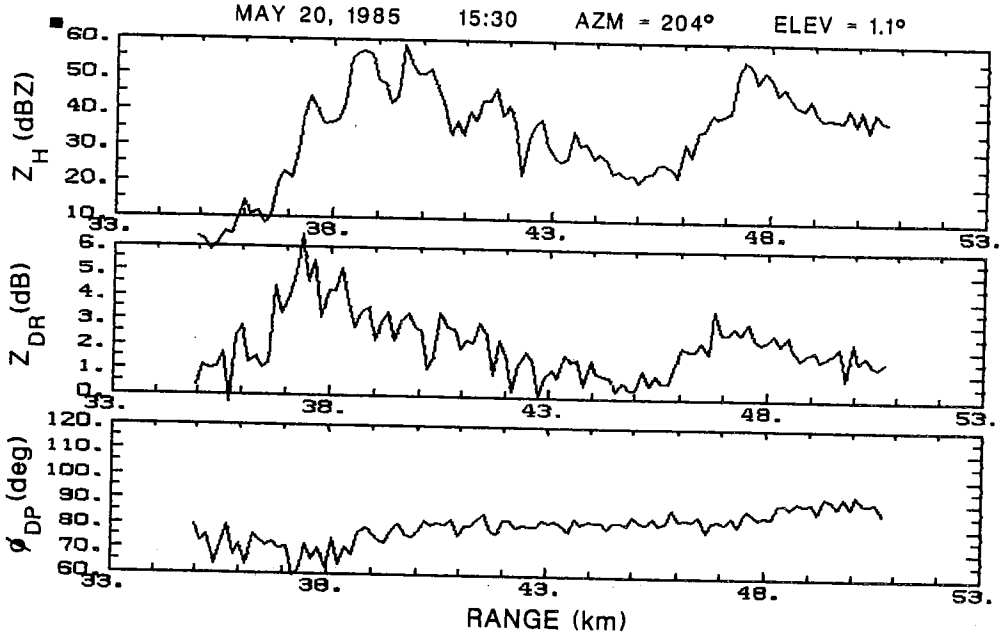
MAY 20, 1985 15:30 AZM = 204° ELEV = 1.1°
Z_H (dBZ)
Z_{DR} (dB)
ϕ_{DP} (deg)
RANGE (km)

(c)

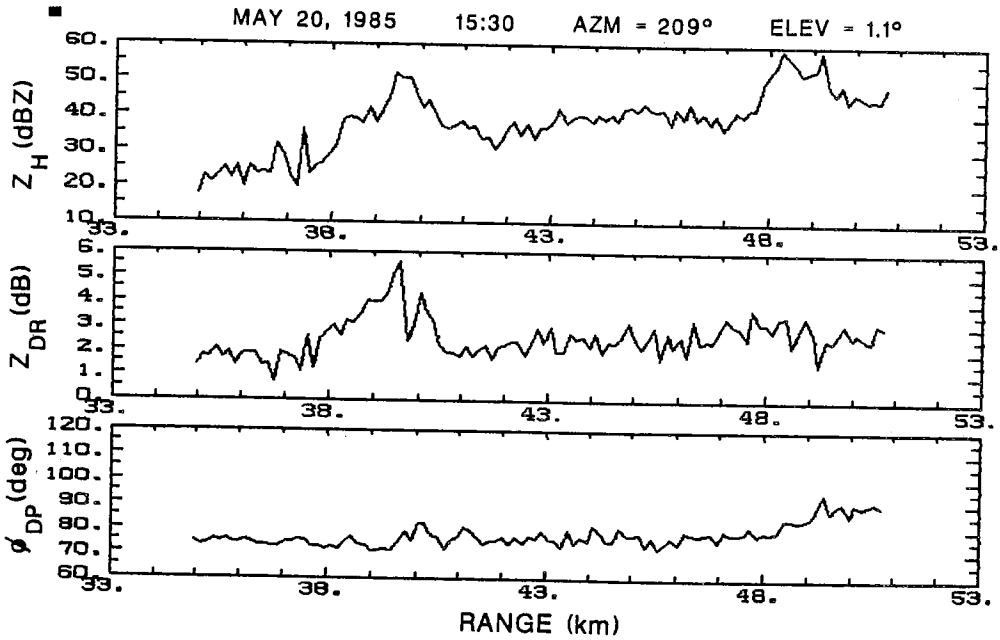
MAY 20, 1985 15:30 AZM = 209° ELEV = 1.1°
Z_H (dBZ)
Z_{DR} (dB)
ϕ_{DP} (deg)
RANGE (km)

(d)

Figure 12

is the total two-way differential propagation phase shift between the radar and the resolution volume. We see that ϕ_{DP} is very noisy, although in the higher reflectivity regions the mean increases monotonically with range. This noise is at times as much as $\pm 5°$. It is also obvious that the side lobe error in $\hat{\phi}_{DP}$ can be reduced by range averaging only when reflectivity is larger than approximately 30 dBZ. At lower reflectivities the error is too large to be removed by smoothing.

4.2. Reflectivity gradient

Fig. (13.a) is a scattergram of the differential reflectivity Z_{DR} versus the reflectivity Z_H data from a single sector scan of an approximately 15 x 15 km area. The data was collected using NSSL's Cimarron radar on May 20, 1985. The scan time is from 15:30:27 to 15:31:46. The azimuth sector is from 192° to 212° and the elevation angle is 1.1°. The data is from the range gates between 35 and 52 km.

The data shows a large scatter; much larger than is expected if the drop size distribution (DSD) were representable by a general gamma DSD with a reasonable variation in the parameters (see: Sachidananda and Zrnić, 1986 for a detailed discussion). The scatter at low reflectivities (< 20 dBZ) may be due to side lobe signal but at higher reflectivities, it is due to DSD variations and the uncertainty in the equilibrium shape of drops. We will not dwell on this aspect of DSD variability any further. More details can be found in the above mentioned reference.

However, we would like to record an observation made during the analysis of the data. While plotting the scattergram from the data, radial by radial as the radar scans, we noticed that all the points in the regions of increasing reflectivity gradient have consistently higher Z_{DR} than for a corresponding reflectivity

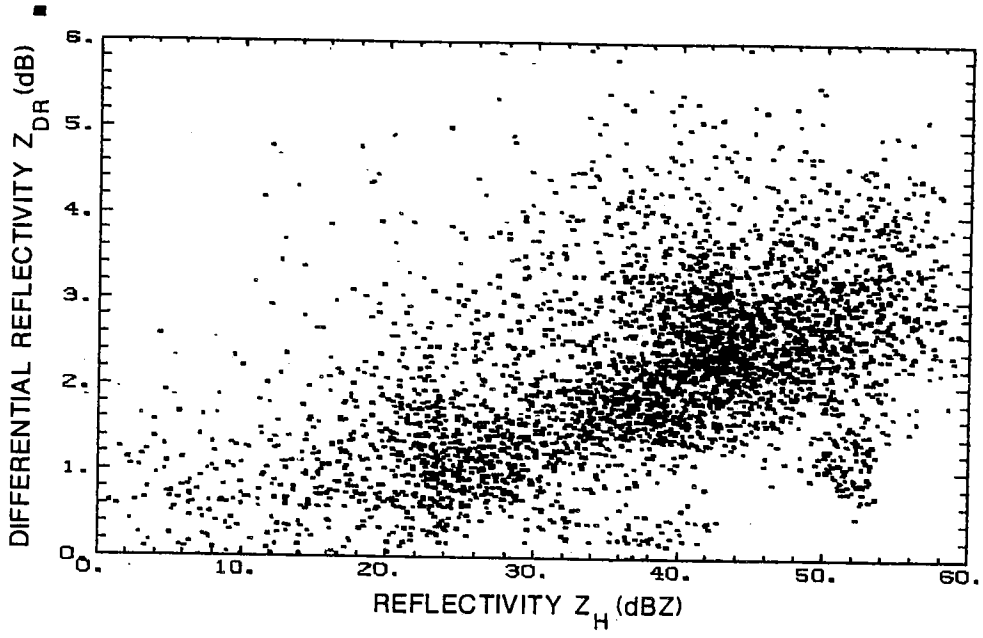

Figure 13(a). Z_{DR} versus Z_H scattergram of data from Cimarron radar. Date: May 20, 1985; time: 15:30:27 to 15:31:46; range: 35 to 52 km; azimuth: 190° to 212°; elevation: 1.1°.

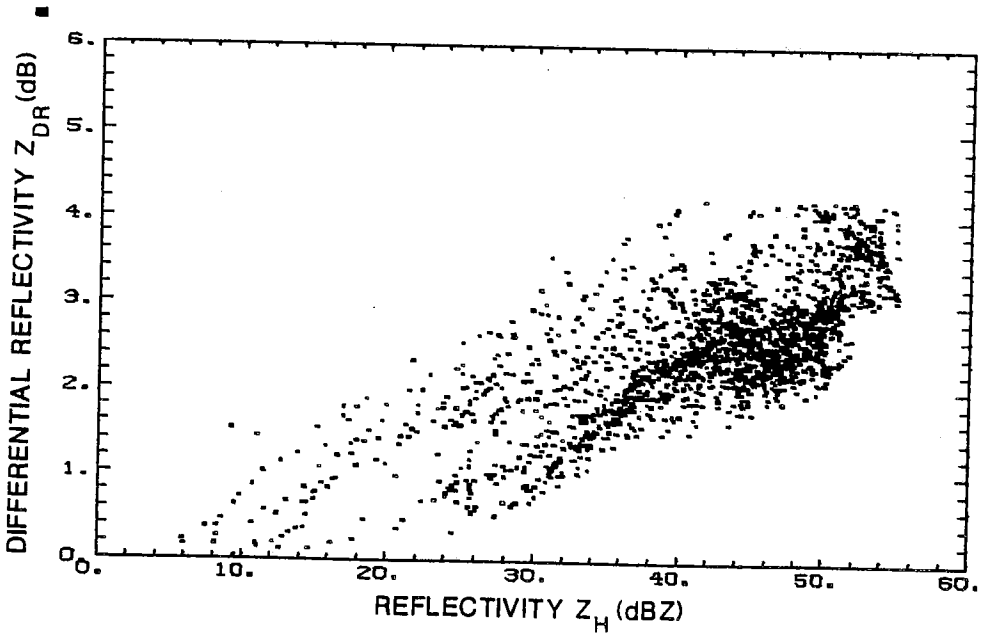

Figure 13(b). Z_{DR} versus Z_H scattergram of radar data from the region of increasing reflectivity gradient. The data is for the same scan as in fig. 13.a.

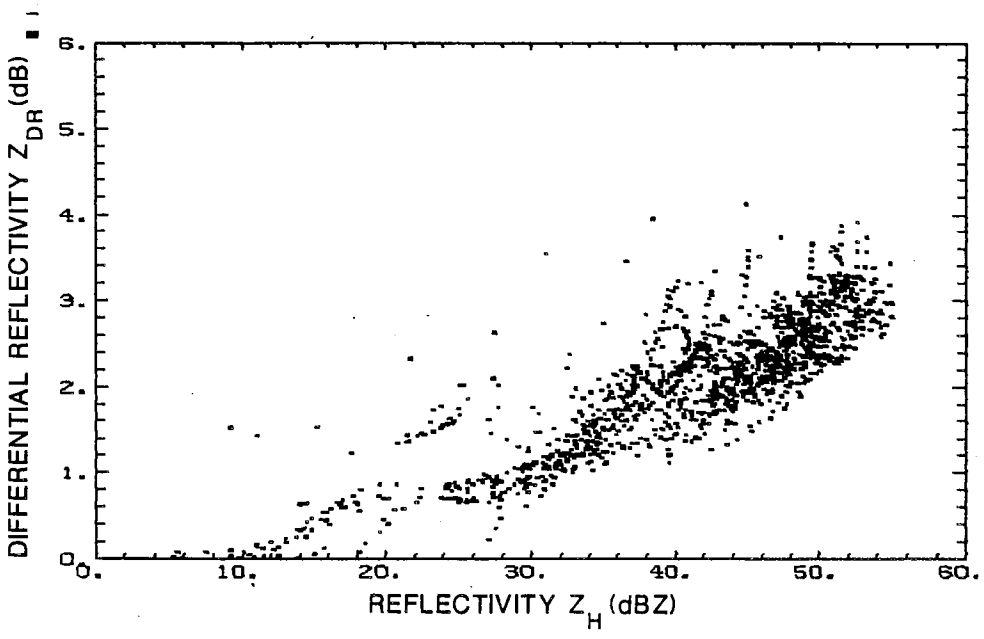

Figure 13(c). Z_{DR} versus Z_H scattergram of radar data from the region of decreasing reflectivity gradient. The data is for the same scan as in fig. 13.a.

in the region of decreasing reflectivity gradient, as seen from the radar along a radial. We have separated these two sets of data in figs. 13.b and 13.c, one from the region of increasing gradient (Fig. 13.b) and the other from the decreasing gradient region (fig. 13.c). The data was smoothed over 16 range gates (2.4 km) to get the pattern more clearly. Although most of the points fall in a common region, a distinct positive scatter only in the increasing reflectivity gradient (fig. 13.b) suggests that the reflectivity gradient has something to do with these higher Z_{DR} values.

A similar but slightly more pronounced effect is observed in the case of differential propagation phase shift constant K_{DP} versus Z_H scattergram. Fig. 14.a is a scattergram of the data from the same storm as in fig (13.a) but taken at an earlier time. The scan time is from 15:13:09 to 15:14:27 and the elevation angle is 0.1°. The data is averaged over 16 gates (2.4 km) before plotting. The next two figures give the same data divided into two regions; increasing reflectivity gradient (Fig. 14.b) and decreasing reflectivity gradient (Fig. 14.c). Here the positive and negative scatter is very clearly shown, although most of the points are in a common region. It is interesting to note that many of the points of large deviation from the mean form a continuous trace and are from individual radials. At low reflectivities (< 30 dBZ) there can be a large scatter due to the side lobe signal, but these individual traces are present even at large reflectivities. The large scatter at lower reflectivities (< 30 dBZ), which is most likely due to the side lobe contamination, also clearly splits into two halves (compare figs. 14.a,b,c). This is puzzling because we would expect the side lobe error to be random.

The causes for the apparent dependency of Z_{DR}, ϕ_{DR} on the reflectivity gradients is not known. It could be that the dynamic process going on inside the storm

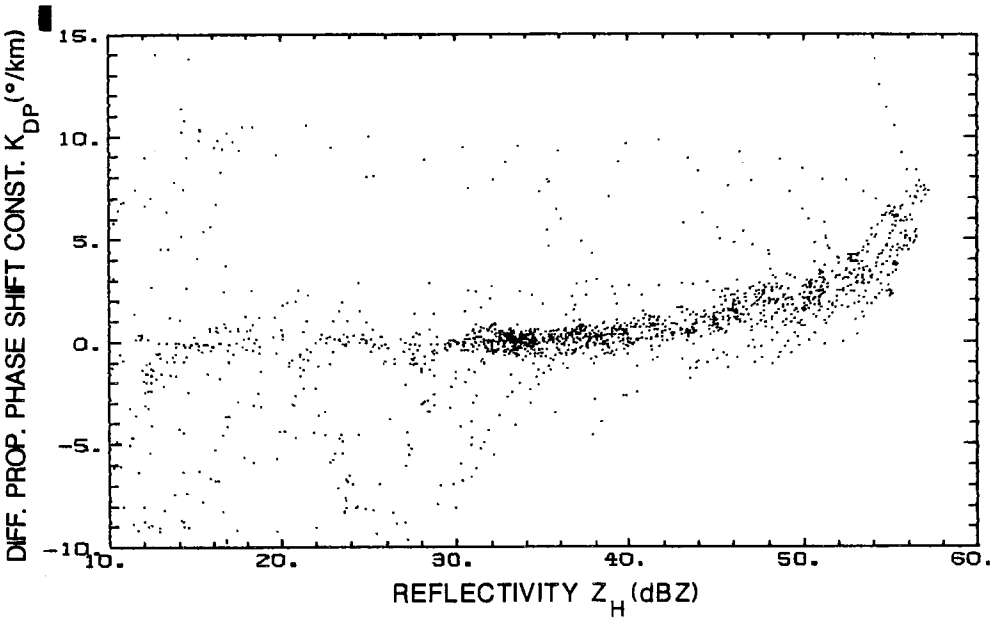

Figure 14(a). K_{DP} versus Z_H scattergram of data from Cimarron radar. Date: May 20, 1985, time: 15:13:09 to 15:14:27; range: 35 to 52 km; azimuth: 192° to 212°; data averaged over 2.4 km in range.

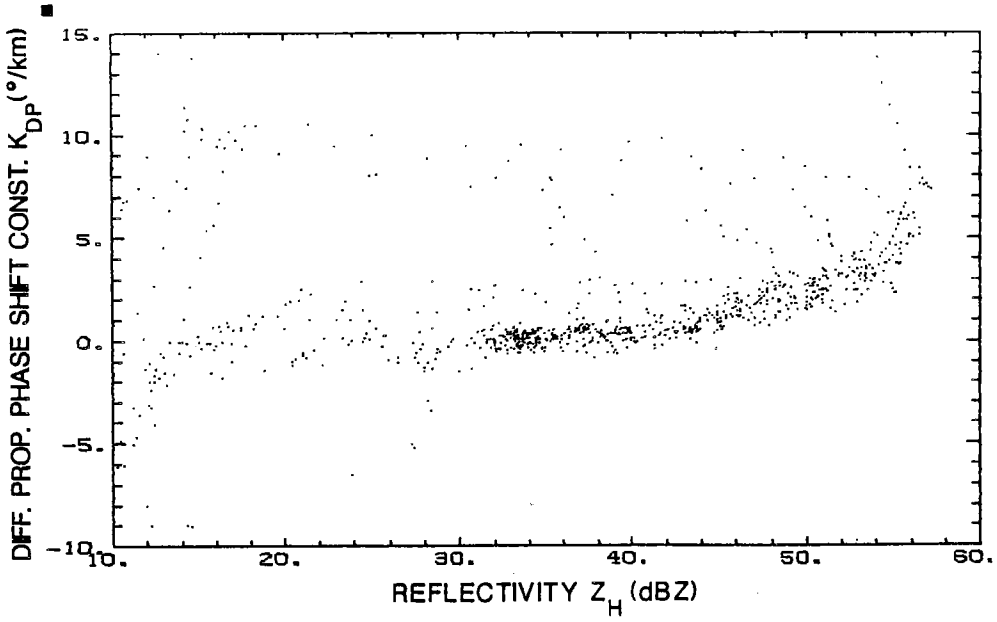

Figure 14(b). K_{DP} versus Z_H scattergram of radar data from the region of increasing reflectivity gradient. The data is for the same scan as in fig. 13.a.

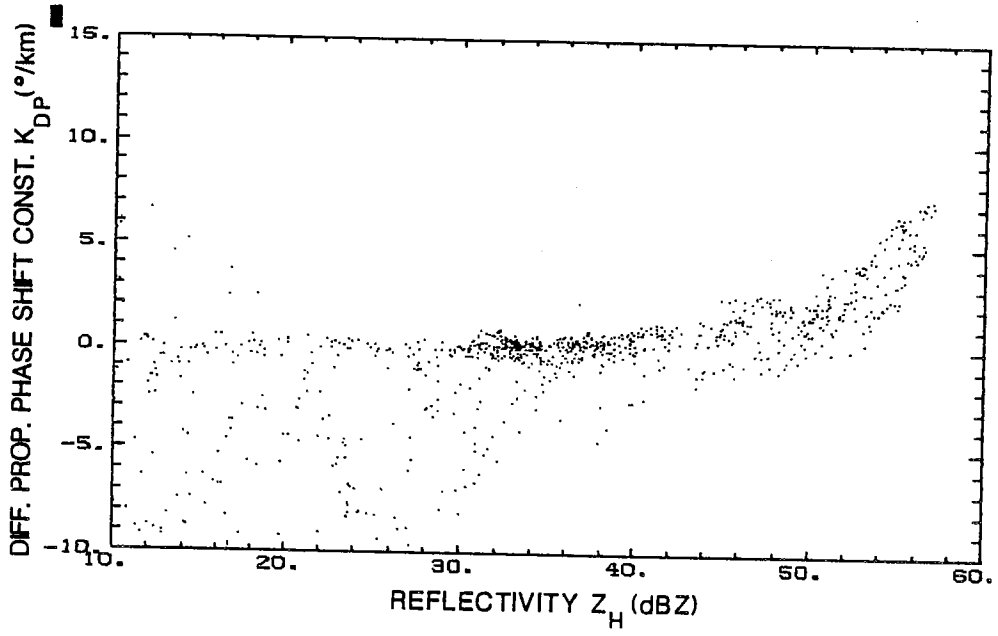

Figure 14(c). K_{DP} versus Z_H scattergram of radar data from the region of decreasing reflectivity gradient. The data is for the same scan as in fig. 13.a.

causes a higher concentration of bigger drops in the leading edge of the storm (NE) than at the trailing edge (SW), thus the Z_{DR} is higher at the leading edge of the storm. Also there could be an equipment anomaly that we are not aware of.

To determine which cause is responsible for the observed gradient effect, we need to collect and analyze data from leading and trailing edges of storms at opposite aspect angles. Unfortunately, all the records presently available are in one category, Z_H increasing with range in the leading and decreasing in the trailing edge.

4.3. Time series records:

Radar data recorded on May 20, 1985 contained 256 sample time series with alternate polarization switching. Each of these samples is a complex number with in-phase (I) and quadrature (Q) components, the quantity $(I^2 + Q^2)$ being proportional to the instantaneous echo power.

In Figures (15.a,b,c,d) are plots of the normalized magnitude of the sample power (normalization is with respect to the peak) against sample number. The x-axis also represents time in number of PRT's (PRT = 768 μs). Note that the two curves for H and V polarization closely follow each other in shape which shows that the correlation coefficient between H and V samples $|\rho_{HV}(0)|$, for zero time lag is near unity (Sachidananda and Zrnić (1985) predict $|\rho_{HV}(0)|^2 \sim 0.995$). The rate of fluctuation of the echo sample power can be used to estimate the decorrelation time and the spectrum width of the signal.

One interesting observation from these time series plots is that there are small cyclical perturbations, with period of about 7 ms, which are out of phase in H and V samples (Figs. 15a,d). These show up only in a few records; in most of the records we have examined the periodic out of phase perturbation was very small or absent. This almost periodic out of phase perturbation is significant in Fig 15.a.

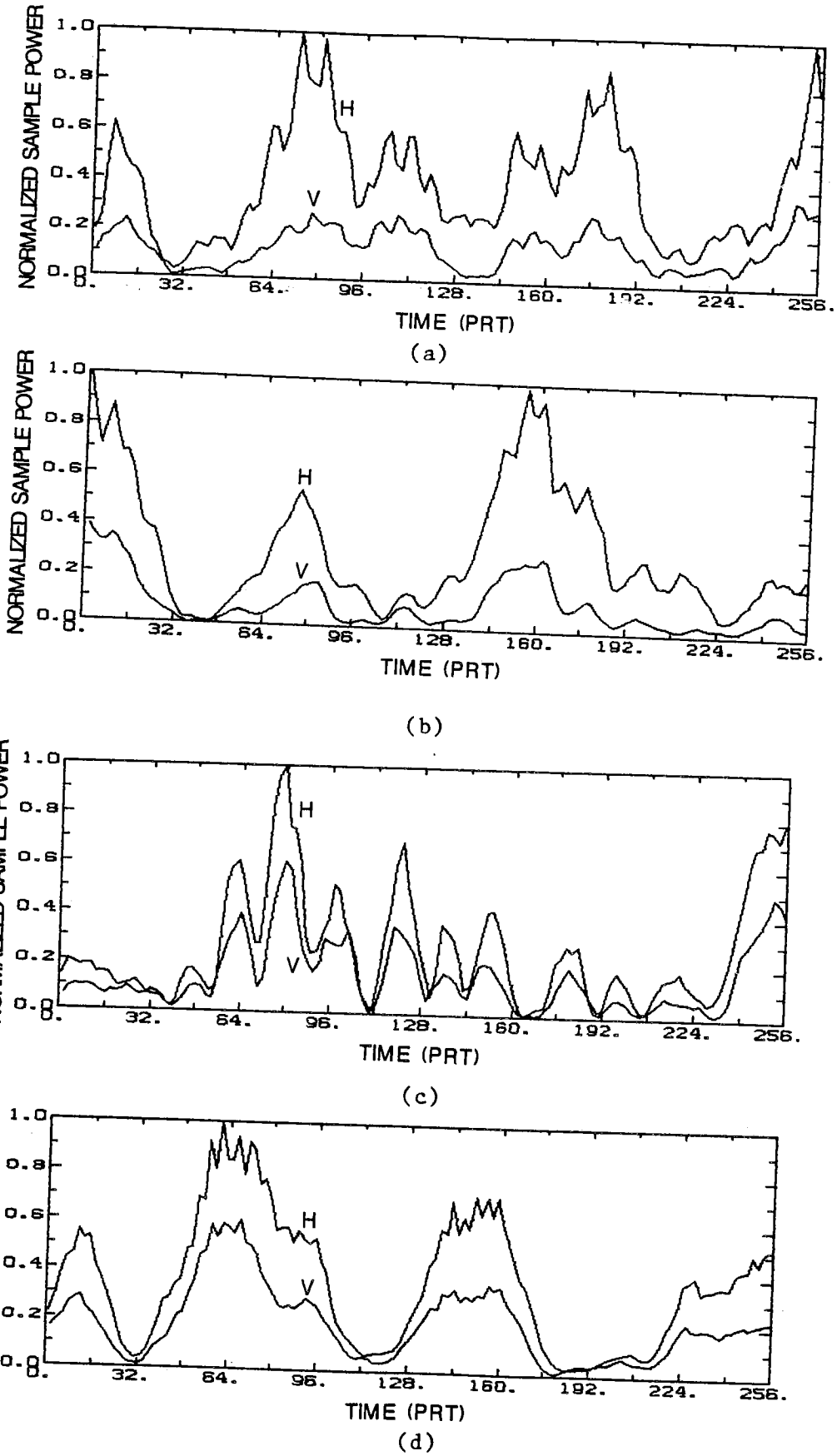

Figure 15. Time series sample power ($I^2 + Q^2$) versus sample number. Sample powers are normalized with respect to the maximum sample power. Time scale is in units of pulse repetition time which is 768 μs.

To get a clearer picture of these perturbations we have plotted $|H|^2/|V|^2$ versus time in figures (16.a to 16.d). The sample powers $|H|^2$ and $|V|^2$ are aligned in time by interpolation. Although there are random perturbations in each of these plots which are due to the statistical nature of the signal itself, a pronounced periodic perturbation is seen in fig. 16.a. The remainder of the figures do not strongly show such behavior, though there is some suggestion of it in some of them. For the data in fig. 16.a the reflectivity Z_H = 32 dBZ and the Z_{DR} = 4.1 dB. Note that the large peaks in fig. 16.a are mostly in the region where H and V signal amplitudes are near zero thus, do not contain significant power (compare fig. 16.a with fig. 15.a). The combination of Z_H = 32 dBZ and Z_{DR} = 4.1 dB seems to be unusual. The data is from the leading edge of the storm where these combinations were predominant. Although there were many more data sets which have unusually high Z_{DR} values at low reflectivity, the pronounced out of phase oscillatory behavior was found only in a few. In fig. 16.a the osillatory amplitude is as much as 2.5 dB peak to peak in the instantaneous Z_{DR}. There is also a significant third harmonic of the fundamental, almost in a definite phase relationship with the fundamental.

In the following we have tried to give a possible explanation to the observations recorded above, but it should not be taken as conclusive. It is pointed out that we have examined only a few time series records and to arrive at any definite conclusion, extensive analysis is required.

The combination of Z_H = 32 dBZ and Z_{DR} = 4.1 dB suggest an extreme form of drop size distribution, possibly caused by drop sorting. A general gamma DSD with a reasonable perturbation in the parameters would not be able to give such large Z_{DR}. Supposing the drop sorting has caused a monosize DSD, we would need a drop size of approximately 6 mm to get a Z_{DR} = 4.1 dB, assuming equilibrium drop shape

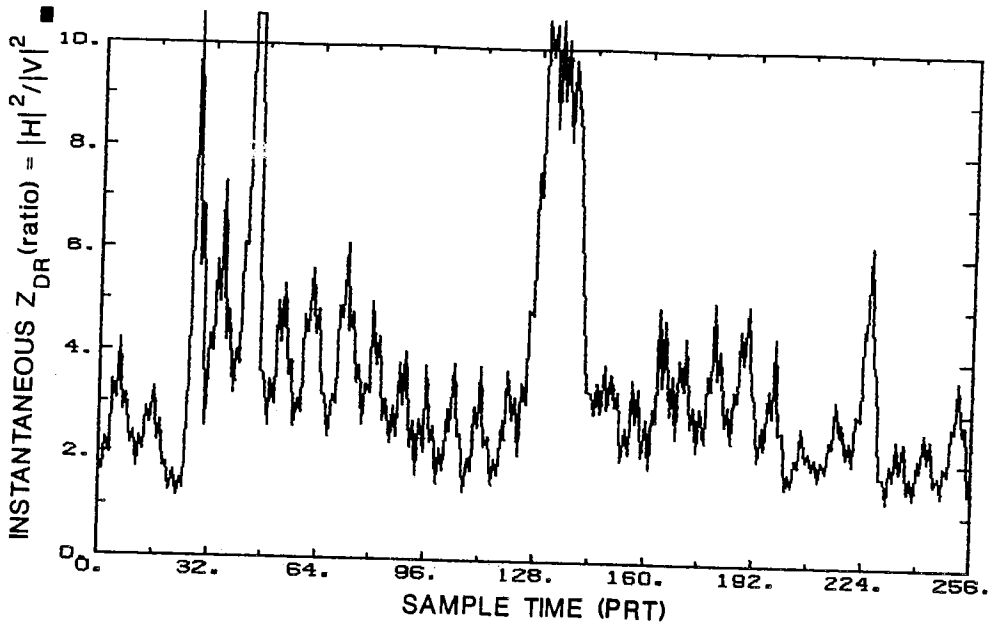

(a)

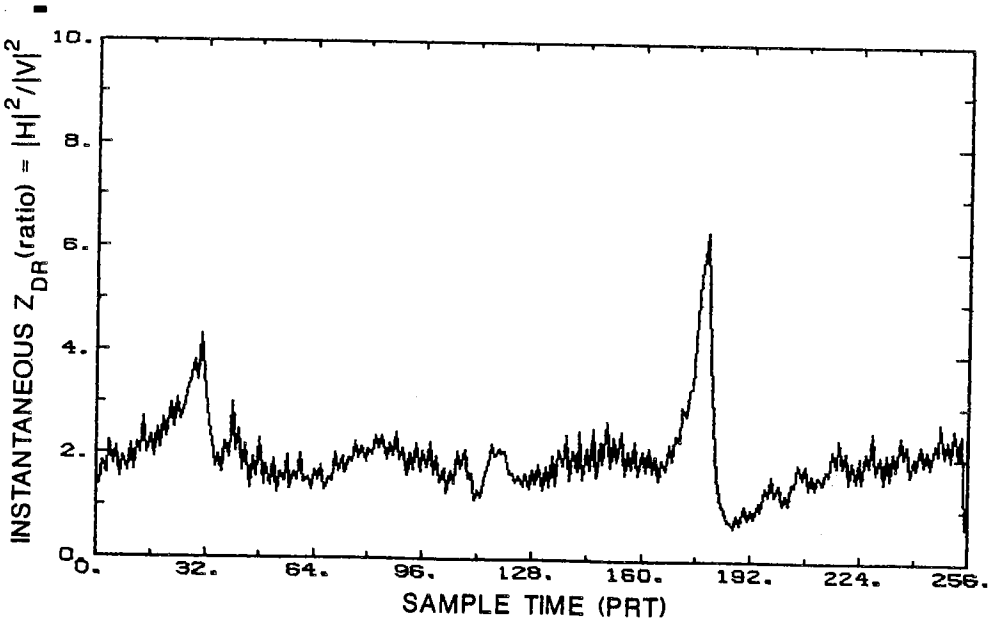

(b)

Figure 16. Variation of the instantaneous $Z_{DR}(\text{ratio}) = |H|^2/|V|^2$ with time; sample powers are aligned in time by interpolation.

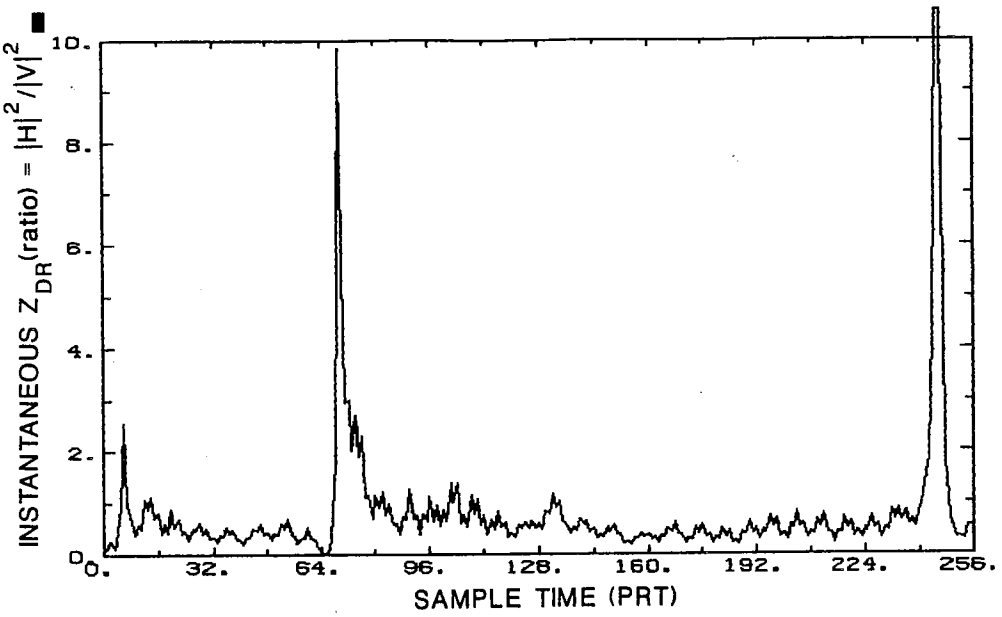
INSTANTANEOUS Z_{DR}(ratio) = $|H|^2/|V|^2$
10.
8.
6.
4.
2.
0.
0.
32.
64.
96.
128.
160.
192.
224.
256.
SAMPLE TIME (PRT)

(c)

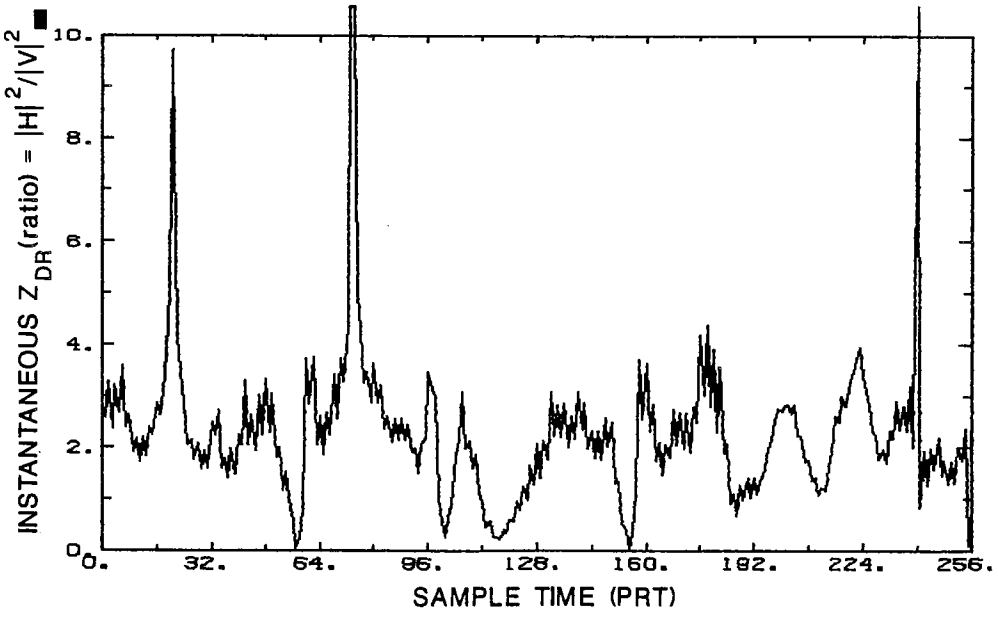
INSTANTANEOUS Z_{DR}(ratio) = $|H|^2/|V|^2$
10.
8.
6.
4.
2.
0.
0.
32.
64.
96.
128.
160.
192.
224.
256.
SAMPLE TIME (PRT)

(d)

Figure 16.

(b/a = 1.5). One of the reported measurements of axis ratios (Chandrasekhar et. al. 1984) suggests that the drops are more oblate than the equilibrium shape; axis ratio can be as high as 1.5 even for 4 mm diameter drops.

The osillatory behavior of Z_{DR} with time can be associated with a synchronous drop oscillation; although we do not know how this synchronism is brought about. The natural oscillations in the drops are likely to have completely random phase, thus would tend to reduce Z_{DR} to some extent. Beard et. al. (1982) show that the mean axis ratios in the presence of drop oscillations are less than the equilibrium axis ratios. We can think of a hypothetical situation capable of inducing synchronous oscillations, wherein the resolution volume contains highly stressed drops due to electric field and a lightning discharge suddenly removes this electric field. For such an excitation all the drops would tend to start oscillating in synchronism but each size drop with its own natural oscillating frequency, thus we would observe a spectrum of oscillations in the instantaneous Z_{DR} versus time plot unless the drops tend to be monodispersed.

If the above hypothesis were true, and asuming the drops are of the same size and oscillate in the fundamental mode, we can use the Rayleigh formula to obtain the drop diameter D_e:

$$f_d^2 = \frac{2}{\pi^2} \frac{T}{\rho} \frac{n(n-1)(n+2)}{D_e^3} \qquad (40)$$

where surface water tension T = 72.75 gr s^{-2} and density ρ= 0.992 gr cm^{-3}. f_d is oscillation frequency (in our case 143 Hz) and n=2 is the mode number. Substitution of these values into (40) produces a drop size of D_e = 1.8 mm. However, from the Z_{DR} value we would get a D_e = 4 mm, which is more than twice the value obtained from the oscillation frequency. Obviously, there is some unexplainable discrepancy which needs further analysis. Although higher mode oscillations could reconcile this discrepancy we do not have a physical reason to accept them.

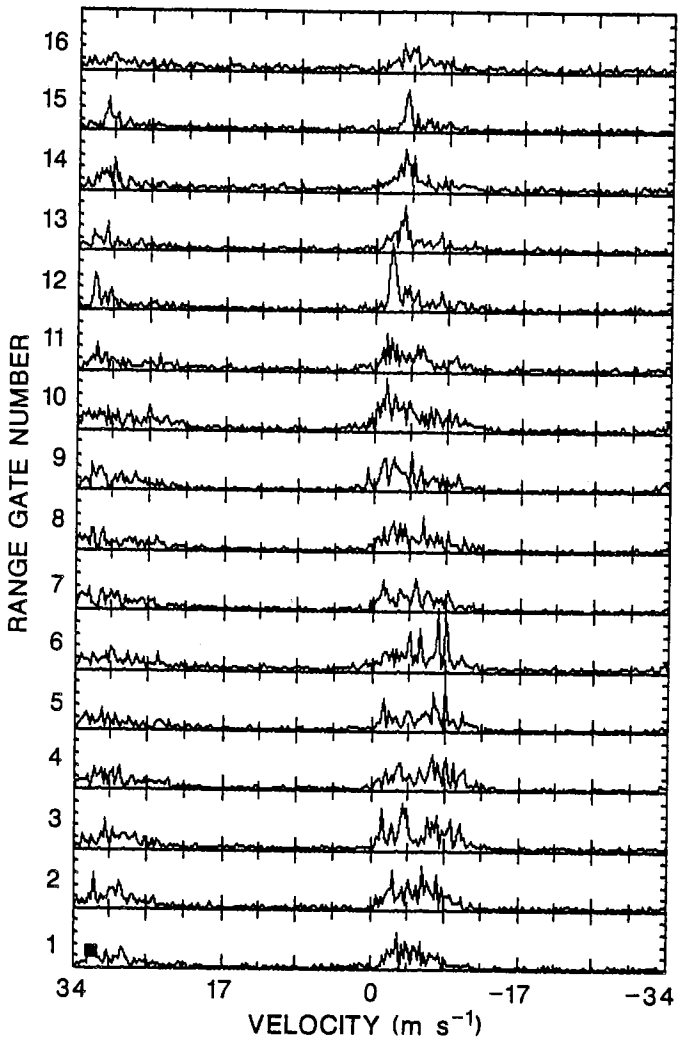

(a)

Figure 17. 16 Spectra of radar signals which have alternating polarization and are from consecutive range locations. The magnitudes of Fourier coefficients are plotted on a linear scale (arbitrary units).

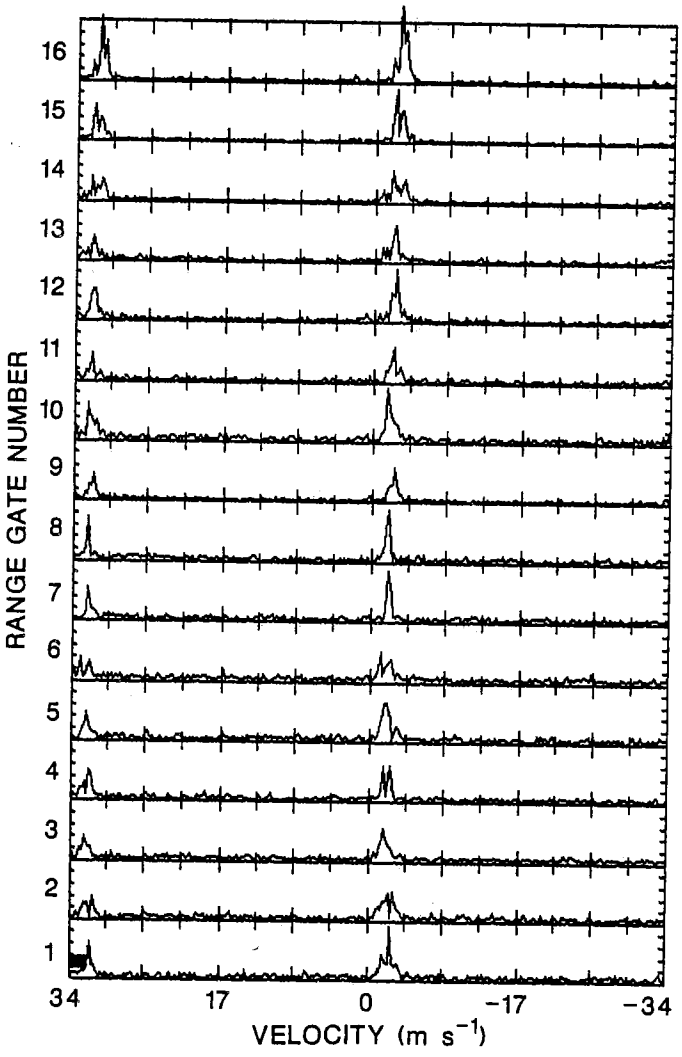
RANGE GATE NUMBER
16
15
14
13
12
11
10
9
8
7
6
5
4
3
2
1
34
17
0
-17
-34
VELOCITY (m s^{-1})

Figure 17(b).

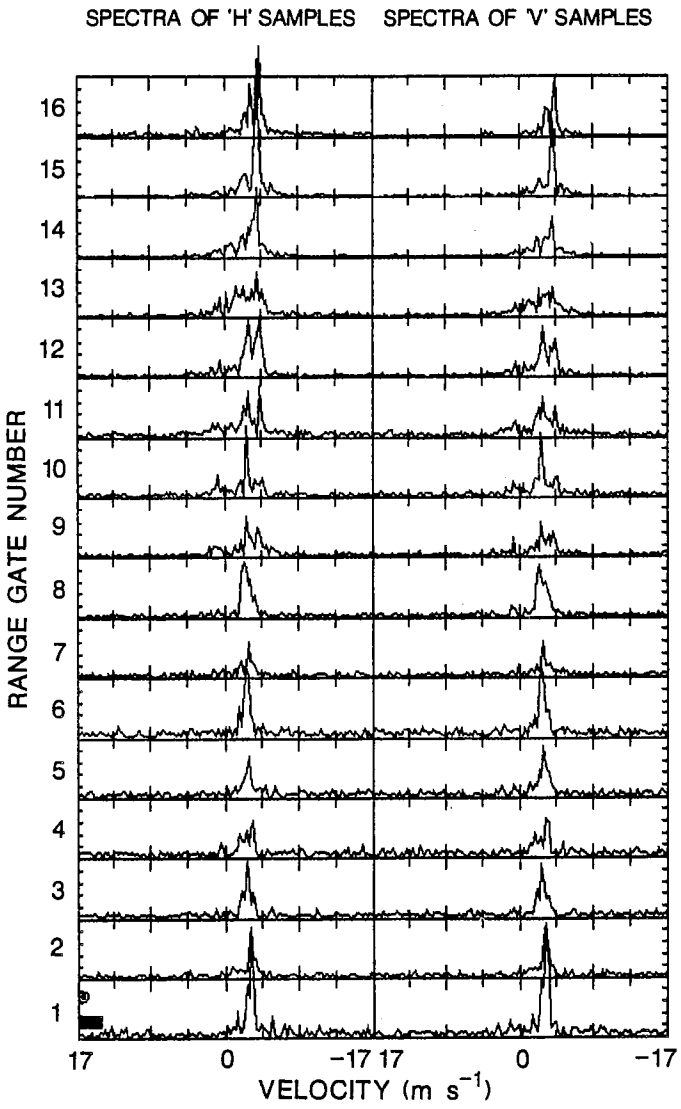

Figure 18. Separate spectra of horizontally and vertically polarized signals. H and V spectra for each of the 16 consecutive range gates are shown side by side.

4.4. Spectra of radar signal with alternating polarization:

Figures (17.a) and (17.b) show some typical spectra. The time series consists of 256 samples with alternate H and V polarizations. Each plot consists of spectra for 16 consecutive range gates spaced 150 m apart along a radial. The vertical axis is the magnitude of Fourier coefficients in arbitrary units. Although each spectrum contain 256 discrete lines, we have joined the tips of the lines for clarity. The horizontal axis is shown as ± 34 m s^{-1} velocity scale.

The effect of amplitude (due to the Z_{DR}) and phase (due to the ϕ_{DP}) modulation is seen clearly as two peaks in the spectra separated by the Nyquist velocity. Note also the remarkable similarity in the shape of the two halves of the spectra. Some of the noisy spectra are from low reflectivity regions of the storm. The similarity in the shape of the positive and negative halves are disturbed in some spectra due to the presence of noise.

We have also given some spectra of H and V samples taken separately in Fig. (18). The two spectra are plotted side by side for each gate. Note that the Nyquist interval for each of the sample sequences is half that for the combined time series. Because of the high correlation between H and V samples, the two spectra have nearly identical shapes, except for the magnitude difference. However, in some spectra we can find minor differences, which are probably due to the side lobe signal. If the antenna patterns for the two polarizations are not matched exactly, the side lobe signal in the two polarizations will be from different regions of the storm, hence can be different.

5. Conclusions

This technical note discusses the estimation of the radar observables from the time-series data of a dual polarized radar with alternate polarization switching. Most of the analysis concerns the modifications in the existing signal

method of a single polarized radar, necessitated by the incorporation of the polarization switching capability. Apart from the three conventional radar observables, viz., reflectivity, velocity and spectrum width, two other radar observables, the differential reflectivity and the differential propagation phase shift, are included in the proposed modified signal processing scheme. The latter two parameters are specific to the radar that alternates the polarization of its transmitted fields.

Section 4 is, for most part, a compilation of several observations made from the first time series recordings of the NSSL's Cimarron radar, modified for dual polarized operation. We have tried to give some explanations for the observations, wherever possible. But, it is emphasized that they are only tentative and should not be taken as conclusive. Extensive analysis of the data is required in several cases to ascertain the validity of the explanations, and perhaps the observations too! However, we hope that this technical note would aid in identifying some areas for further investigations.

6. References

Beard, K.V., D.B. Johnson and A.R. Jameson, 1982: "Raindrop distortion", Proceedings, Symposium on Multiple-Parameter Radar Measurements of Precipitation, URSI, Bournemouth, U.K.

Bringi, V.N., T.A. Seliga, and S.M. Cherry, 1983: "Statistical properties of the dual polarization differential reflectivity (Z_{DR}) radar signal", IEEE Trans. Geosci. Remote Sens., GE-21, 215-220.

Chandrasekhar, V., V.N. Bringi and J. Vievekanandan, 1984: "Estimation of raindrop axial ratios using orthogonally mounted 2D-PMS precipitation probes during MAYPOLE", Conf. Volume, 22nd Conf. on Radar Meteorology, AMS, Zurich, Switzerland, pp. 322-326.

Doviak, R.J. and D.S. Zrnić, 1984: "Doppler Radar and Weather Observations", Academic Press, 458 p.

Johnson, D.B., 1984: "The Effect of Antenna Side Lobes on Multi-Parameter Radar Measurements", J. Atmospheric and Oceanic Tech. 1, pp. 287-290.

Sachidananda, M. and D.S. Zrnić, 1985: "Z_{DR} measurement consideration for a fast scan capability radar". Radio Science, 20, pp. 907-922.

Scahidananda, M. and D.S. Zrnić, 1986: "Differential propagation phase shift and rainfall rate estimation", Radio Science, 21, pp. 235-247.

Seliga, T.A. and V.N. Bringi, 1976: "Potential use of radar differential reflectivity measurements at orthogonal polarizations for measuring precipitation". J. Appl. Meteorol., 15 pp. 69-76.

Zrnić, D.S., 1977: "Spectral moment estimates from correlated pulse pairs." IEEE Trans. on Aerospace Electronic Systems AES-13, pp. 344-354.

Zrnić, D.S., 1979: "Estimation of spectral moments for weather echoes", IEEE Trans. on Geoscience and Remote Sensing, GE-17, pp. 113-128.

CIMMS Reports and Contributions List

1. "Collection of Lecture Notes on Dynamics of Mesometeorological Disturbances". Proceedings of CIMMS Symposium on Dynamics of Mesometeorological Disturbances, May 12-16, 1980, edited by Yoshi K. Sasaki, Nobutaka Monji and Steve Bloom, July 1980, 431 pp.

2. "Laboratory Studies of Tornado Vortices". Nobutaka Monji, September 1980, 62 pp.

3. "The Structure of the Convective Boundary Layer over Urban Terrain". Randolph J. Evans and A. SundarRajan, March 1981, 3 pp.

4. "Correlation of Doppler Radar Velocities and Reflectivities with Application to Retrieving the Transverse Wind". Glenn Richard Smythe, May 1981, 72 pp.

5. "Variational Analysis/Forecast Cycling Based on the Conservation of Potential Vorticity". John M. Lewis, May 1981, 40 pp.

6. "Nonhydrostatic Axisymmetric Hurrican Model". Hugh E. Willoughby, September 1981, 16 pp.

7. "A Variational Initialization Assimilation Scheme: Basic Concept and Preliminary Result". Yoshi K. Sasaki, March 1982, 19 pp.

8. "A Survey of Applications of the Finite-Element Method to Meteorological Models". Y.K. Sasaki and L.P. Chang, March 1982, 45 pp.

9. "Use of the Inequality Constraint in Adjusting Superadiabatic Layers". Yoshi K. Sasaki and John McGinley, Mon. Wea. Rev., Vol. 109, No. 1, 1981, 194-196.

10. "Observation of Steady Glow and Multicolored Flashes Associated with a Thunderstorm". John McGinley, Conrad Zielger and Diane Ziegler, Bull. Amer. Meteor. Soc., Vol. 63, No. 2, 1982, 189-190.

11. "A Doppler Analysis of Squall-Line Convection". Cathy J. Kessinger, Carl E. Hane and Peter S. Ray, Preprint of 12th Conference on Severe Local Storms. January 12-15, 1982, San Antonio, Tx.

12. "The Gust Front". Chapter IX of E. Kessler edited Thunderstorms: A Social, Scientific, & Technological Documentary Vol. 2, Thunderstorm Morphology and Dynamics, February 1982, by Y.K. Sasaki and Tom Baxter, pp. 281-296.

13. "The Evolution of an Oklahoma Dryline, Part I: A Meso- and Subsynoptic-Scale Analysis". John McCarthy and Steven E. Koch, Journ. Atm. Sci., Vol. 39, No.3, 1982, 225-236.

14. "The Evolution of an Oklahoma Dryline, Part II: Boundary-Layer Forcing of Mesoconvective Systems". Steven E. Koch and John McCarthy, Journ. Atm. Sci. Vol. 39, No. 3, 1982, 237-257.

15. "Doppler Radar Observations of Momentum Flux in a Cloudless Convective Layer with Rolls". R.M. Rabin, R.J. Doviak and A. Sundara-Rajan, Journ. Atm. Sci., Vol. 39, No. 4, 1982, 851-863.

16. "A Wintertime Mesoscale Cold Front in the Southern Plains". Howard B. Bluestein, Bull. Amer. Meteor. Soc., Vol. 63, No. 2, 1982, 851-863.

17. "Retrieval of Microphysical and Thermal Variables in Observed Sonvective Storms". Conrad L. Ziegler and Peter S. Ray, Preprint of Cloud Physics Conference, Nov. 15-18, 1982, Chicago, IL.

18. "Methods in Numerical Weather Prediction: Where Finite-Element Methods Stand?". Y.K. Sasaki and L.P. Chang, Finite Element Flow Analysis, University of Tokyo Press, July 1982, Tokyo, Japan, pp. 27-33.

19. "A Diagnosis of Alpine Lee Cyclogenesis". John McGinley, Mon. Wea. Rev., Vol. 110, No. 9, 1982, 1271-1287.

20. "A Comparison of Techniques to Estimate Vertical Velocities and Drop Size Spectra". Karen L. Sangren and Peter S. Ray, Preprint of Cloud PHysics Conference, Nov. 15-18, 1982, Chicago IL.

21. "Comparison of Doppler Radar Measurements to the Simulation of Deep Moist Convection in an Axisymmetric Cloud Model". Phillip D. Bothwell, Carl E. Hane and Peter S. Ray, December 1982, 105 pp.

22. "A General Formalism of Variational Analysis". F.X. LeDimet, December 1982, 35 pp.

23. "An Analysis of the Relation between Doppler Spectrum Width and Thunderstorm Turbulence". Michael J. Istok, May 1983, 81 pp.

24. "Satellite Data Assimilation Using NASA Data Systems Test 6 Observations". Y.K. Sasaki and J.S. Goerss, Mon. Wea. Rev., Vol. 110, No. 11, 1982, 1635-1644.

25. "Development of a Two-Dimensionsl Finite-Element PBL Model and Two Preliminary Model Applications". L.P. Chang, E.S. Takle and R.L. Sani, Mon. Wea. Rev., Vol. 110, No. 12, 1982, 2025-2037.

26. "Anti- Clockwise Rotation of the Wind Hodograph. Part I: Theoretical Study". M. Kusuda and P. Alpert, Journ. Atm. Sci., Vol. 40, No. 2, 1983, 487-499.

27. "Horizontal Components of the Frictional Force in the Sigma Coordinate System for Mesometeorological Flow Models". P. Alpert and J. Neumann, Preprint of 6th Conference on Numerical Weather Prediction, June 6-9, 1983, Omaha, Nebr.

28. "On Numerical Solution of Vertical Structure Functions in Normal Mode Method". Y.K. Sasaki and L.P. Chang, Preprint of 6th Conference on Numerical Weather Prediction, June 6-9, 1983, Omaha, Nebr.

29. "Proceedings of the NEXRAD Doppler Radar Symposium/Workshop" September 22-24, 1982, edited by Peter S. Ray and Keven Colbert, May 1983, 235 pp.

30. "Parameterization of the Surface Fluxes of Heat and Momentum for the Convective Atmospheric Boundary Layer". A. Sundara-Rajan and I. Runge, Arch. Met. Geop. Biocl., Ser. A, Vol. 32, 1983, 23-24.

31. "The Parameter Estimation Problem for Parabolic Equations in Multidimensional Domains in the Presence of Point Evaluations". K. Kunisch and L. White, March 1983, 58 pp.

32. "Annual Report 1982". Yoshi K. Sasaki, Cooperative Institute for Mesoscale Meteorological Studies, May 1983, 41 pp.

33. "Collection of Lecture Notes on Mesoscale Models". Proceedings of CIMMS Symposium on Mesoscale Modeling, June 1-2, 1982, edited by Yoshi K. Sasaki, Sharon Ray and L.P. Chang, May 1983, 315 pp.

34. "An Oklahoma Squall Line: A Multiscale Observational and Numerical Study". Cathy J. Kessinger, Peter S. Ray and Carl E. Hane, July 1983, 211 pp.

35. "Parameter Estimation for Elliptic Equations in Multidimensional Domains with Point and Flux Observations". K. Kunisch and L. White, August 1983, 49 pp.

36. "Surface Meteorological Observations in Severe Thunderstorms Part II: Field Experiments with TOTO". Howard B. Bluestein, Journ. Appl. Meteor., Vol. 22, No. 5, 1983, 919-930.

37. "Associated Lightning Discharges". Vladislav Mazur, Geophys. Research Letters, Vol. 9, No. 11, 1982, 1227-1230.

38. "The Effect of Polarization on Radar Detection of Lightning". Vladislav Mazur, Geophys. Research Letters, Vol. 9, No. 11, 1982, 1231-1234.

39. "A Comparison of Techniques to Estimate Vertical Air Motions and Raindrop Size Distributions". Karen L. Sangren and Peter S. Ray, September 1983, 137 pp.

40. "Dynamic Initialization with Filtering of Gravity Waves". F.X. LeDimet, Y. Sasaki and L. White, September 1983, 12 pp. Printed 8-84.

41. "Precipation Variability in Oklahoma". Don Fred and Edwin Kessler, September 1983, 57 pp.

42. "Correlation Analysis of Doppler Radar Data and Retrieval of the Horizontal Wind". G.R. Smythe and D.S. Zrnic, Journ. Clim. Appl. Meteor. Vol. 22, No. 2, 1983, 297-311.

43. "Hail Growth in an Oklahoma Multicell Storm". C.L. Ziegler, P.S. Ray and N.C. Knight, Journ. Atmos. Sci., Vol. 40, No. 7, 1983, 1768-1791.

44. "Measurements in the Vicinity of Severe Thunderstorms and Tornadoes with TOTO: 1982-1983 Results". Howard B. Bluestein, Preprint of 13th Conference on Severe Local Storms, October 17-20, 1983, Tulsa, Okla.

45. "Multiple-Doppler Radar network Design". Peter S. Ray and Karen L. Sangren, Journ. Clim. Appl. Meteor., Vol. 22, No. 8, 1983, 1444-1454.

46. "Lightning and Related Phenomena in Thunderstorms and Squall Lines". Vladislav Mazur et al., Paper presented at the AIAA 22nd Aerospace Sciences Meeting, January 9-12, 1984, Reno Nevada, No. AIAA-84-0467.

47. "Conditions for Lightning Strikes to an Airplane in a Thunderstorm". Vladislav Mazur et al., Paper presented at the AIAA 22nd Aerospace Sciences Meeting, January 9-12, 1984, Reno Nevada, No. AIAA-84-0468.

48. "A Synoptic and Photographic Climatology of Low-Precipitation Severe Thunderstorms in the Southern Plains". Howard B. Bluestein and Carlton R. Parks, Monthly Wea. Rev., Vol. 111, No. 10, 1983, 2034-2046.

49. "Four-Dimensional Satellite Data Assimilation". Y. Sasaki and James S. Goerss, January 1984, 94 pp.

50. "Lightning Flash Density versus Altitude and Storm Structure from Observations with UHF- and S-band Radars". Vladislav Mazur, John C. Gerlach and David W. Rust, Geophysical Research Letters, Vol. 11, No. 1, 61-64.

51. "Estimation of Parameters in Nonlinear Flow Equations with Discontinous Solutions". L.W. White, March 1984, 32 pp.

52. "Retrieval of Thermal and Microphysical Variables in Observed Convective Storms". Conrad L. Ziegler, April 1984, 198 pp.

53. "A Simulation of Lake Michigan's Winter Land Breeze on 7 November 1978". P. Alpert and J. Newmann, Mon, Wea. Rev., Vol. 111, No. 10, 1983, 1873-1881.

54. "An Early Winter Subtropical Cyclone in the Eastern Mediterranean". P. Alpert, Israel Journ. Earth-Sciences Vol. 33, 1984, 150-156.

55. "Estimates of Correlation Functions in Time and Space Derived from Oklahoma Thunderstorms Surface Data". Kevin E. Kelleher and Ken W. Johnson, October 1984, 174 pp.

56. "Variational Assimilation of Single Doppler Radar Observation to Produce Three Dimensional Wind Field." Y.K. Sasaki, 1984. (as of 3-12-86, not finished. Still being revised and will be submitted later. Not printed, bound or published)

57. "Methods in Numerical Weather Prediction- Where Finite Element Methods Stand?" by Y.K. Sasaki and L.P. Chang, Finite Elements in Fluids Vol. 5 John Wiley and Sons, Limited, 1984.

58. "Lightning Locations Related to Storm Structure in Supercell and Multicell Storms." Lisa Walters Rasmussen, Peter S. Ray and William Taylor, January 1985, 117 pp.

59. "Kinetic Energy Evolution in a Developing Severe Thunderstorm." Keith A. Brewster, February 1985, 148 pp.

60. "On the Enhanced Smoothing Over Topography in Some Mesometeorological Models." by Pinhas Alpert and J. Neumann, Boundary-Layer Meteorology Vol. 30 D. Reidel Publishing Co., 1984, 293-312.

61. "On Numerical Solution of the Vertical Structure Equation in the Normal Mode Method." by Y.K. Sasaki and L.P. Chang, Mon. Wea. Rev. May 1985 Vol. 113, No. 5, pp.782-793.

62. "Variational Mesoscale Satellite Data Assimilation and Initialization". Y.K. Sasaki and James Goerss, NASA Grant No. NAG%-289. May 1985, 71 pp.

63. "Annual Report 1983". Y.K. Sasaki, Cooperative Institute for Mesoscale Meteorological Studies, October 1985, 13 pp.

64. "Annual Report 1984". Y.K. Sasaki, Cooperative Institute for Mesoscale Meteorological Studies, October 1985, 16 pp.

65. "Analysis of Airborne Doppler Lidar, Doppler Radar, and Tall Tower Measurements of Atmospheric Flows in Quiescent and Stormy Weather". H.B. Bluestein, R.J. Doviak, M.D. Eilts, E.W. McCaul, R. Rabin, A. Sundara-Rajan, D.S. Zrnic; NASA Grant No. NAS8-34749. June 1985, 165 pp.

66. "The Relationship of Divergent Outflow Magnitude at Upper Storm Levels as Measured by Doppler Radar to Hailstorm Intensity and Tornadoes". Arthur Witt, June 1985, 69 pp.

67. "A Mesocyclone and Tornado-Like Vortex Generated by the Tilting of Horizontal Vorticity: A Laboratory Simulation". Lans P. Rothfusz, September 1985, 106 pp.

68. "Second Order Modeling of the Planetary Boundary Layers" Tsan-Hsing Shih and J.L. Lumley, January 1986. 39 pp.

69. "Nonlinear Circulations in a Symmetrically Unstable Flow". Qin Xu, Journ. Atm. Sci., Vol. 43, No. 5, March 1986, 494-498.

70. "Storm Top Divergence from Single Doppler Velocity Fields and its Relationship to Storm Intensification and Severity". Ritchie Eyster, June 1986, 108 pp.

71. "Characteristics of Echoes from Alternately Polarized Transmission". by M. Sachidananda and D. S. Zrnic, July 1986. 54 pp.